AN ABSTRACT OF THE THESIS OF

Mohammed AL-Mulhim for the degree of Master of Science in Chemical Engineering presented on September 8, 1995.

Title : Enhancement of Mass Transfer Coefficient in a Magnetically Stabilized Liquid-Solid Fluidized Bed.

Redacted for Privacy

Abstract approved : _____
Goran Jovanovic

Previous studies in Magnetically Stabilized Fluidized Bed, MSFB, did not offer experimental evidence of the actual enhancement of the mass transfer coefficient in MSFB over that in conventional fluidized bed. No relationship was established between mass transfer coefficient, the fluid flow characteristics, and magnetic properties of MSFBs.

In this study, we experimentally confirmed the enhancement of the mass transfer coefficient in MSFB by using the adsorption of methylene blue dye on ferromagnetic particles. Under different experimental conditions the mass transfer coefficient is enhanced up to 75%. This is accomplished primarily due to the influence and change of the fluid interstitial velocity, $u_{int} = u_0/\varepsilon$. The fluid interstitial velocity, which is a measure of the fluid-particle relative velocity, is substantially improved by the application of the magnetic field. The relationship which describes the average bed porosity as a function of magnetic field intensity and fluid superficial velocity is

established. A linear adsorption isotherm relating the equilibrium concentrations of MB in the solution to the amount of MB adsorbed on the ferromagnetic particles is also obtained.

A mathematical model is developed and solved analytically to evaluate the mass transfer coefficient obtained in our experimental system. The equation which represents our experimental system and is used to calculate the mass transfer coefficient is,

$$\mathrm{Ln}\left\{\frac{C\,(1+mK_e)-C_0}{C_0(1+mK_e)-C_0}\right\}=\frac{1+mK_e}{mK_e}\frac{F}{V}\left(e^{-\alpha k}-1\right)t$$

An equation is proposed which correlates the obtained values of the mass transfer coefficient (Sherwood number, Sh) with the fluid interstitial velocity (modified Reynolds number, Re′). The proposed correlation is

$$\mathrm{Sh}=\frac{0.0365}{\varepsilon}\mathrm{Re'Sc}^{0.33}$$

where

$$\mathrm{Re'}=\frac{\rho u_0 d_p}{\mu\varepsilon}$$

The porosity of the MSFB is calculated from the equation,

$$\varepsilon=\varepsilon_{ms}+(\varepsilon_{ff}-\varepsilon_{ms})\exp\left(-(1-\varepsilon)(\alpha H+\beta)\frac{H}{H_{ms}}\right)$$

which was proposed by Honorez (1994), and fits our experimental data satisfactorily.

Enhancement of Mass Transfer Coefficient in a Magnetically Stabilized Liquid-Solid Fluidized Bed

by

Mohammed AL-Mulhim

A THESIS

submitted to

Oregon State University

in partial fulfillment of
the requirement for the
degree of

Master of Science

Completed September 8, 1995

Commencement June 1996

Master of Science thesis of Mohammed AL-Mulhim presented on September 8, 1995

APPROVED :

Redacted for Privacy

Major Professor, representing Chemical Engineering

Redacted for Privacy

Chair of Department of Chemical Engineering

Redacted for Privacy

Dean of the Graduate School

I understand that my thesis will become part of the permanent collection of Oregon State University libraries. My signature below authorizes release of my thesis to any reader upon request.

Redacted for Privacy

Mohammed AL-Mulhim

TABLE OF CONTENTS

TABLE OF CONTENTS (Continued)

TABLE OF CONTENTS (Continued)

LIST OF FIGURES

LIST OF FIGURES (Continued)

LIST OF TABLES

LIST OF APPENDIX FIGURES

LIST OF APPENDIX TABLES

NOMENCLATURE

a	Surface area of particles	$[\ cm^2\ ]$
A	MB absorbance	[%]
A_0	MB initial absorbance	[%]
a'	Surface area of particles per volume of column	$\left[\frac{cm^2(particles)}{cm^3(column)}\right]$
C	Methylene blue (MB) conc. in water	[mg/ml]
C_r	MB conc. in particle pores at radius, r	[mg/ml]
C_s	MB equilibrium conc.	[mg/ml]
C_{ss}	MB conc. at steady state	[mg/ml]
C_0	MB initial conc.	[mg/ml]
d_p	Average particle diameter	[mm]
D	MB diffusivity in water	$[\ cm^2/s\ ]$
F_b	Buoyancy force exerted on a particle	[N]
F_d	Drag force exerted on a particle	[N]
F_g	Gravitational force exerted on a particle	[N]
g	Gravitational acceleration	$[\ m/s^2\ ]$
Ga	Galileo number = $\frac{d_p^3 \rho \Delta \rho g}{u^2}$	[/]
H	Magnetic field intensity	[A/m]

H_{ms}	Magnetic field intensity at the transition between the partially stabilized and stabilized fluidization regime	[A/m]
I	Electric current intensity	[A]
k	Liquid-solid mass transfer coefficient	[cm/s]
K_e	Adsorption equilibrium constant	[ml/ g of particles]
L	Overall bed height	[cm]
L_i	Probe location	[cm]
L_0	Height of the packed bed	[cm]
m	Mass of particles per unit volume of particle free bed	[g/cm^3]
M	Magnetization	[A/m]
n	Solenoid tuns	[turns/m]
N	MB Conc. adsorbed on particles	[g of MB/ g of particles]
P_i	Pressure in the i^{th} probe	[Pa]
P_t	Pressure at the top of the bed	[Pa]
r	Radial position	[mm]
R	Electric current resistance	[Ω]
Re	Reynolds number = $d_p u\rho / \mu$	[/]
S	Slope evaluated from equation 5-4	[1/s]
Sc	Schmidt number = $\mu / \rho D$	[/]
Sh	Sherwood number = kd_p / D	[/]
t	Time	[s]
u_0	Liquid superficial velocity	[cm/s]

u_{int}	Interstitial velocity = u_0/ε	[cm/s]
u_{mf}	Minimum fluidization velocity	[cm/s]
U	Voltage applied across the solenoid	[V]
V	Volume of particle -free liquid in bed	[cm^3]
W	Mass of particles	[g]

GREEK SYMBOLS

β	Constant in equation 3-2	[/]
α	Coefficient in equation 3-15 , ($\alpha = a'V/F$)	[s/cm]
α	Constant in equation 3-2	[m/A]
ΔP	Pressure drop across the bed	[Pa]
ΔP_i	Pressure drop between i^{th} probe and the top of the bed	[Pa]
ε	Average bed porosity	[/]
ε_{ff}	Bed porosity without magnetic field	[/]
ε_{mf}	Bed porosity at minimum fluidization, (H=0)	[/]
ε_{ms}	Average bed porosity at the transition between the partially stabilized and stabilized fluidization regime	[/]
ε_0	Porosity of the packed bed	[/]
μ	Fluid viscosity	[Pa.s]
ρ	Liquid density	[kg/m^3]
ρ_p	Particle density	[kg/m^3]
χ	Particle magnetic susceptibility	[/]

Enhancement of Mass Transfer Coefficient in a Magnetically Stabilized Liquid-Solid Fluidized Bed

CHAPTER 1
INTRODUCTION

Magnetically Stabilized Fluidized Bed (MSFB) is one of the most recent and novel chemical engineering development in the area of fluid-solid contacting operations. It combines some of the best characteristic of fluidized bed, like low pressure drop and the ability to transport solid throughout the system, with excellent efficiency of the fixed bed in mass transfer, heat transfer, and chemical conversion.

Fluid- particle mass transfer in fluidized beds is a very important transport phenomenon in many chemical engineering operations such as adsorption, desorption, drying, ion exchange, and evaporation.

Numerous studies, Filippov (1960), Rosensweing (1979), Arnaldos et al.(1985), and Burns et al.(1988) were conducted to investigate the fluid dynamic characteristics of the MSFB. Only some of them, Casal et al.(1991), and Honerez (1994) predicted that the magnetic field may enhance the mass transfer coefficient between fluid and particles.

Researchers in biotechnology have already applied the MSFB in some industrial bioprocesses. Soda et al.(1981), have studied the performance of immobilized enzymes in the MSFB. Also, continuous affinity chromatography and bioseperations

using the MSFB has been investigated by Burns and Graves (1985,1986). Terranova and Burns (1990) have also studied a processing of cell suspensions in the MSFB. Even though these studies have demonstrated that their process operations have been improved by using the MSFB, experimental evidence were not offered to show the actual enhancement of mass transfer coefficient over that of a normal fluidized bed. Moreover, no correlation between the bed viodage, which is affected by the magnetic field intensity, and the mass transfer coefficient was established.

The main objective of this work is to study the effect of the magnetic field on the mass transfer coefficient between water and ferromagnetic particles in MSFB. To accomplish this objective, the following tasks have to be accomplished :

1- design and construction of the experimental apparatus,

2- production of ferromagnetic particles,

3- collection of experimental data on the effect of magnetic field intensity on bed viodage (porosity), and

4- development of a mathematical model to calculate the mass transfer coefficient for the adsorption of methylene blue dye on the ferromagnetic particles.

Finally, we will formulate an empirical correlation that will relate mass transfer coefficient, Sherwood number (Sh), to the MSFB flow properties (Re, Sc, ε).

CHAPTER 2
EXPERIMENTAL APPARATUS

The experimental apparatus used in this study is shown schematically in Figure 2-1. The apparatus consists of the following elements :

1- Fluidization column,

2- Fluidizing particles,

3- Water supply system,

4- Instrumentation, and

5- Magnetic field generator.

2.1 Fluidization Column

The Plexiglas column is designed to support all experimental needs and, at the same time, is easy to disassemble and reassemble whenever needed. The column consists of four main sections:

Fliudization Section: This section is a 735 [mm] long tube that has an internal diameter of 62.5 [mm]. At the bottom of this section, a circular distributor is bolted to the wall of the tube.

The distributor is a 4 [mm] thick perforated Plexiglas plate 75.5 [mm] in diameter which has two hundred 2 [mm] circular holes. The plate is covered with a plastic wire-mesh screen which prevents particles from penetrating through the plate holes.

Figure 2-1 : Experimental apparatus

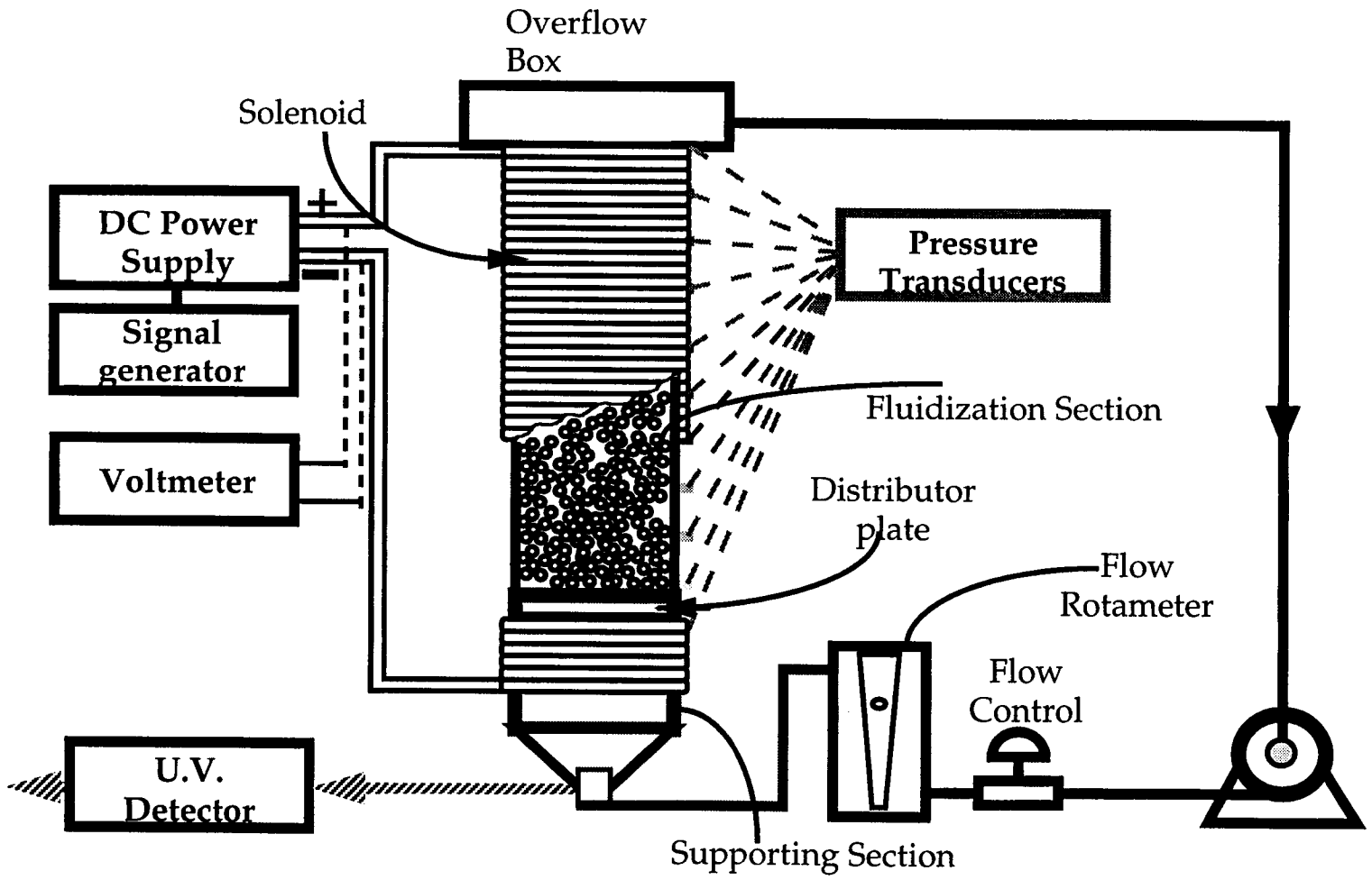

On the top of this section is a 15 [mm] thick supporting ring glued on the outside wall of the fluidization column. The ring is supporting the overflow box, which is described below.

Supporting Section : This section is an 85 [mm] long tube that has exactly the same diameter as the fluidization column. Its main purpose is to support the fluidization section. The sealing between the two sections of the fluidization column is provided by an o-ring.

Column Base : The base consists of two plates that have the same wall thickness, 11.5[mm]. The top plate is glued to a 75.5 [mm] diameter supporting column that provides extra support to the fluidization column. The bottom plate is bolted to two supporting wooden plates that can be adjusted to provide a vertical alignment to the column. The wooden plates are mounted on metal bars that are firmly fixed to the wall.

Overflow Box : A 2900 [cm^3] Plexiglas box is used as the water overflow section. The box is bolted to the supporting ring that is fixed on the fluidization column. A rubber circular gasket is mounted on top of the supporting ring to prevent any potential leak during the column operation. The inlet to the overflow box is covered by a metal screen to prevent any escaped particle from leaving the column, hence, protecting the recirculating water supply system.

2.2 Fluidizing Particles :

2.2.1 Production of Particles

The particles used in this study are composite ferromagnetic particles which are made of alginate beads mixed with ferromagnetic powder. The device used for preparation and production of the particles is schematically shown in Figure 2-2.

Figure 2-2 : Particles production schematic diagram

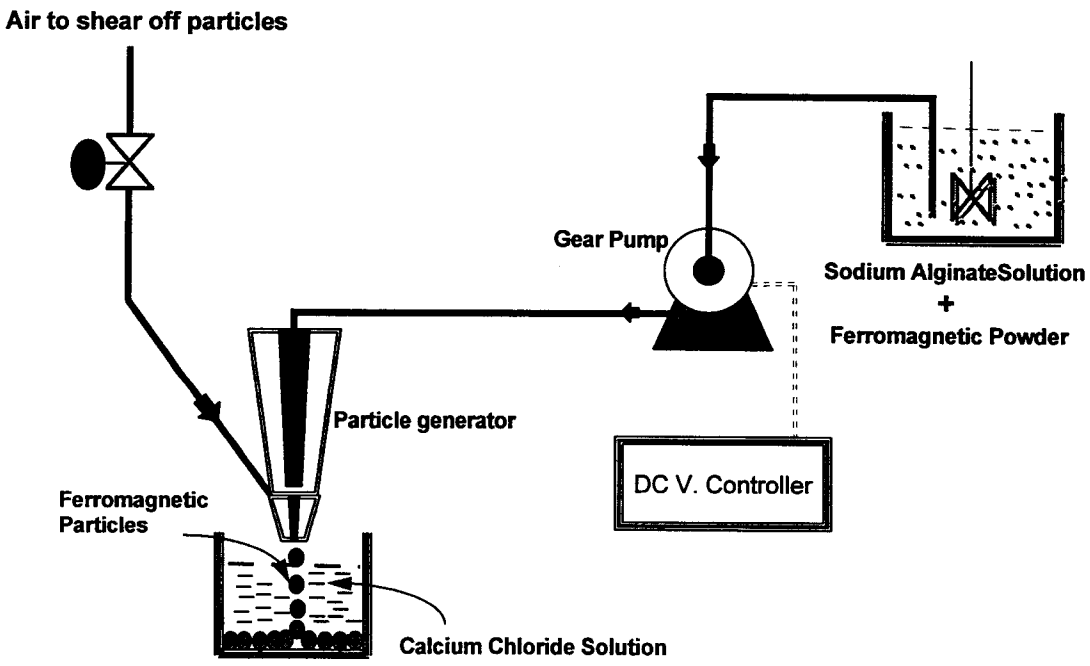

It consists of the following :

Ferromagnetic Alginate Solution : A 2 % (by weight) solution of high viscosity (Kelton HV donated by Kelco Co.) sodium alginate in water is prepared beforehand, and then, the ferromagnetic powder is added, 20 % by weight. This mixture is prepared according to the procedure described in Appendix A. The properties of the ferromagnetic powder are listed in Appendix B. The solution is mixed continuously, while it is being pumped through the particle generator to prevent powder precipitation from the solution.

DC- Voltage Driven Gear-Pump : A gear pump which is driven by a 24 DC voltage power supply is used to pump the ferromagnetic solution to the particle generator. The gear pump speed is controlled separately by a 0-5 DC V. control knob. The pump discharges the solution into the particle generator via a 1/4" PVC tube.

The Particle Generator : Detailed drawings of the particle generator are shown in Appendix C. The particle size is adjusted by regulating the pressure and the air flow, which is used to shear the particles off the dropper nozzle.

Calcium Chloride Cross-Linking Solution : A 1.0 Molar calcium chloride solution is used to cross link the ferromagnetic sodium alginate droplets coming out of the dropper. Once the droplets are introduced to the calcium chloride solution, almost instantly calcium alginate will form on the surface of the sodium alginate beads and they will maintain their spherical shape which they had when injected into the calcium chloride solution. Initially, the droplet center will be unreacted sodium alginate, but

over a period of time calcium will diffuse into the center and form a complete calcium alginate structure. The reaction between calcium ions and the alginate molecules can be represented by :

$$2Na(Alg) + Ca^{++} \Leftrightarrow 2Ca(Alg_2) + 2Na^{+}$$

The composite ferromagnetic droplets are left in calcium chloride solution for 24 hours before they are ready for use.

During the particles production, the speed of the gear pump is kept constant by keeping the DC V controller at 3.0 [V]. The air source pressure is maintained at 15.0 [psig]. After producing a batch of one half liter of beads, the pump gears have to be cleaned thoroughly and then the pump has to be flushed with fresh water for approximately half an hour. This is to maintain the pump efficiency and hence to make sure that the production rate of the beads are constant.

The produced batches of particles are mixed together and cleaned with fresh water. To determine the particles average diameter, random batches of particles are chosen and then, different samples are taken from each batch. The diameter of each particle in the different samples is measured by a caliper. The particle diameters are found to range between 1.2 and 1.8 [mm].

To make sure that the particle diameters range is consistent for every batch of particles, the minimum fluidization velocity is measured for each batch, and found to be almost identical. Each batch of particles is kept filled with distilled water before being used in the experiments.

2.2.2. Particles Properties :

Particle properties are summarized in Table 2-1.

Table 2-1 : Particles Properties

Mean d_p [mm]	1.5 ±0.3
ρ_p [kg/m^3]	1370
$\varepsilon_{mf,\,exp.}$ [/]	0.375
$u_{mf,exp.}$ [cm/s]	0.68
$u_{mf,\,cal.}$ [cm/s]	0.75
$\chi = \alpha H + \beta$ [/]	0.17

The minimum fluidization velocity is evaluated from the pressure drop-velocity measurements in the fluidization column. Figure 2-3 shows ΔP-u_0 diagram for the particles used in this study.

Figure 2-3: Experimental measurements of the minimum fluidization velocity.

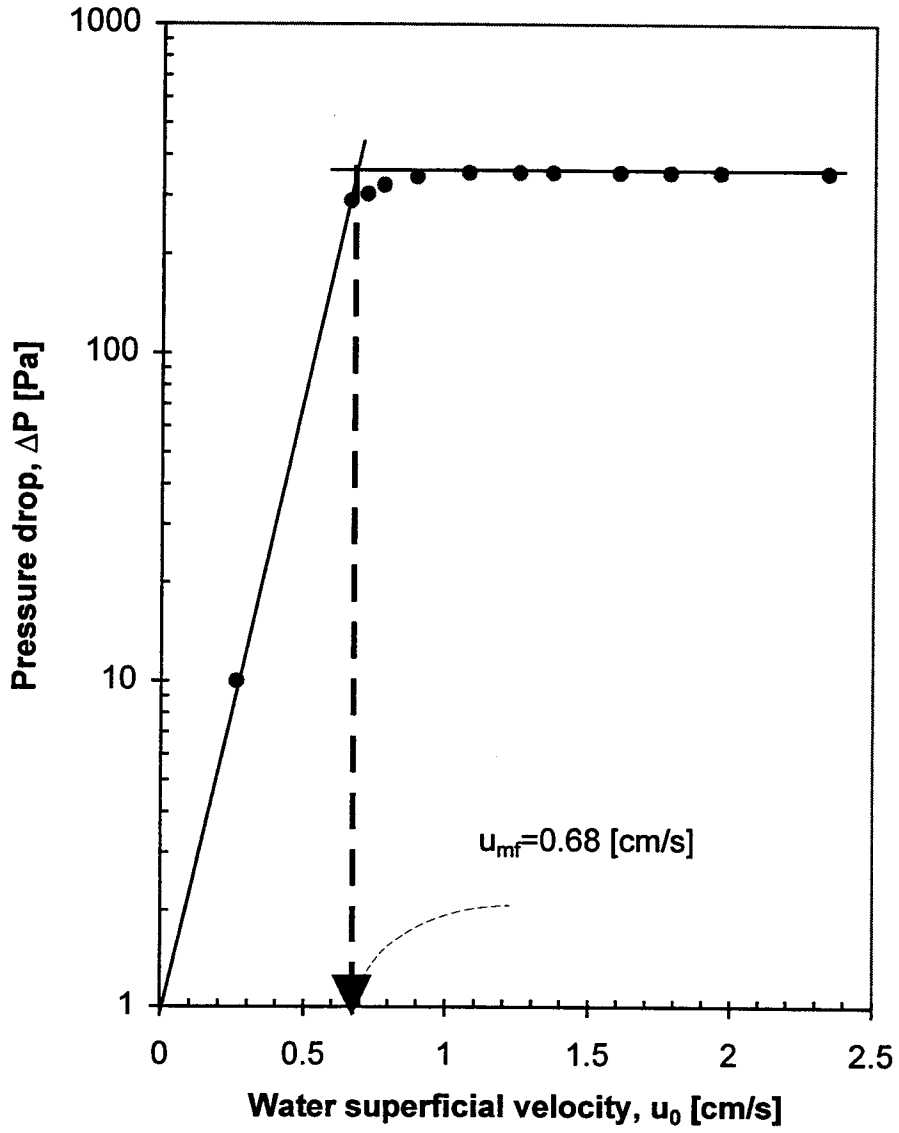

Experimentally obtained u_{mf} matches visual observations and the value estimated from the correlation suggested by Saxena and Vogel (1977) :

$$\frac{u_{mf} d_p \rho}{\mu} = \left\{(25.3)^2 + 0.0571 Ar\right\}^{0.5} - 25.3 \qquad (2\text{-}1)$$

where Ar is Archimedes number and is defined as :

$$Ar = \frac{d_p{}^3 \rho(\rho_p - \rho)g}{\mu^2} \qquad (2\text{-}2)$$

The error between the experimental and estimated value is less than 10%.

An important property of our particles is the magnetic susceptibility χ. Magnetic susceptibility is found to be a linear function of the magnetic field intensity H, Arnaldos et al, (1985).

$$\chi = \alpha H + \beta \qquad (2\text{-}3)$$

The magnetization of particles, M is a linear function of the magnetic field intensity if magnetic susceptibility is assumed to be constant.

$$M = \chi H \qquad (2\text{-}4)$$

otherwise, one can write,

$$M = \alpha H^2 + \beta H \qquad (2\text{-}5)$$

The coefficient β can be evaluated from standard magnetization curves (shown in Appendix D) which display M versus H relationship. β is found from the slope of the

M-H curve at the origin (H=0), a procedure employed previously by Honorez (1994).

$$\frac{dM}{dH} = 2\alpha H + \beta \qquad \Rightarrow \qquad \left[\frac{dM}{dH}\right]_{H=0} = \beta \qquad (2\text{-}6)$$

The magnetization curves for our particles show a linear relationship between M and H, which indicates that the slope at any point is constant. Hence the slope at origin (H=0), is actually the slope of the entire M-H line. The coefficient α in the equation 2-1 is, in all probability, a very small number, as noted previously by Honorez (1994).

Consequently, α can be neglected ($\chi \sim \beta$), especially when H is not very large, which is the case in our experiments. The ferromagnetic powder content of our particles is 20% by weight, which corresponds to a magnetic susceptibility of 0.17 [/].

2.3 Water Supply System :

The water supply system consists of a pump driven by a 1/3 hp. and 1725 rpm. motor. The pump suction is connected to the overflow box via a 3/4" tube. The pump discharge is directed via a 3/4" tube and a flow rotameter to the fluidization column. The pump flow is regulated by a 3/4" ball valve that is mounted upstream of the flow rotameter. The rotameter is calibrated to reflect the rotameter readings with their corresponding water superficial velocities, u_0 in fluidization column. The calibration curve is shown in Appendix E.

3.4 Instrumentation :

Pressure Measuring System : The pressure measuring system consists of a group of twelve 6 mm diameter glass tubes. Each tube is connected to its corresponding pressure port via a 1/4" plastic tube. The pressure ports, which are made of 3/16" copper tubings, are fixed at different locations on the fluidization column wall. Consequently, the pressure at any of the pressure ports is measured by measuring the water level in the glass tubes.

The pressure port locations along the fluidization column wall, with reference to the zero level (the distributor plate), are tabulated in Table 2-2.

Table 2-2 : Pressure port locations along the fluidization column

Port #	Distance [cm]
1	0.75
2	8.2
3	13.2
4	18.2
5	23.2
6	28.3
7	33.5
8	36.3
9	38.6
10	41.3
11	43.6
12	46.3

Ultraviolet (UV) Detector : Methylene blue dye is used as the adsorbate substance in this work. A UV detector is used to measure the UV absorbance of the MB dye. Bear-Lambert law indicates that the UV absorbance is linearly proportional to the concentration of the absorbing material. The UV detector absorbance readings and the corresponding MB concentrations are calibrated. The calibration curve is shown in Appendix E.

MB solution samples are continuously drawn from the experimental apparatus via a 1/16″ diameter and a 3′ long plastic tube, which is installed downstream of the recirculating water pump. Hence, sufficient pressure is provided for the samples to pass through the UV detector with the least possible residence time. The samples are returned to the overflow box if needed.

2.5. The Magnetic Field Generator :

The magnetic field generator consists of two direct current (DC) power supplies connected in series with a copper coil solenoid. The solenoid consists of 91 turns of 1/4" copper tubing that is fixed around a 15 [cm] outer diameter and 80 cm long plastic tube. This is equivalent to 113 turns per meter length of column.

$$n = 113\left[\frac{\text{turns}}{\text{m}}\right] \qquad (2\text{-}7)$$

Each DC power supply could maintain a 0-5 [V] voltage across the solenoid and provide 0-200 [A] of current. Cooling water is passed through the solenoid to prevent it from overheating.

The output voltage of the DC power supplies, and hence the corresponding current through the solenoid, is manually controlled using a voltage control knob. To determine the system resistance, the setting of the power supply was controlled manually, and the voltage readings and their corresponding current readings were recorded. The system resistance was found to be 0.57Ω. The voltage vs. current calibration curve is shown in Appendix E.

The magnetic field intensity H can be calculated according to the following relation :

$$H = In \quad [A/m] \tag{2-8}$$

CHAPTER 3
THEORETICAL BACKGROUND

3.1 Liquid-Solid Mass Transfer Coefficient in Fluidized Beds :

Even though there are no complete experimental studies on liquid-solid mass transfer coefficient in MSFB, numerous studies were performed in ordinary fluidized beds, which could be used as a source of comparison to our work.

Mass transfer coefficient correlations in conventional fluidized beds have been reported by several investigators. For example, Fedrov(1950) determined mass transfer coefficient by measuring the drying rate of particles in fluidized bed. Kettenring(1950) and Shulman and Romankov(1957) determined their mass transfer coefficient correlations by measuring the rate of adsorption and desorption of fluidizing particles . Numerous mass transfer correlations and models for different chemical engineering processes are reported by Upadhyay and Tripathi(1975).

Most of the previous correlations have shown a strong influence of Reynolds number and the bed porosity on the mass transfer coefficient (Sherwood number). For example, the following correlations are reported by Fan et al (1960) and Coderc et al (1972) respectively :

$$Sh = 2 + 1.51(1-\varepsilon)Re^{0.5}Sc^{0.33} \qquad (3\text{-}1)$$

$$Sh = \frac{0.054}{\varepsilon^2} ReSc^{0.33} \qquad (3\text{-}2)$$

Surprisingly, some researchers, Riba and Couderc (1980), Ballesteros et al (1982) have reported a very weak dependence, or a complete absence of correlation between mass transfer coefficient, fluid velocity (Reynolds number), and bed porosity. Their correlations are in contradiction with most of previous investigations and they will not be considered as references to our work.

Table 3-1 summarizes the existing correlations between liquid-solid mass transfer coefficient (Sh) and the fluidization conditions (Re, Sc, ε), obtained for conventional fluidized beds.

The only way to enhance mass transfer coefficient in a conventional fluidized bed, (for a particular type and size of particles) is to increase the fluid velocity, u. However, an increase in fluid velocity will result in increased bed porosity ε. In other words, u and ε are coupled and have opposite and competing effects. This means that the fluid interstitial velocity ($u_{int.} = \frac{u}{\varepsilon}$), which is the relative velocity between the fluid and the fluidizing particles, may not change at all. Hence, the mass transfer coefficient, which depends primarily on $u_{int.}$, will stay the same or even decrease.

Another problem normally encountered in a conventional fluidized bed is the elutriation of fluidized particles when the fluid velocity approaches terminal velocity of particles. This could be resolved by extending the height of the fluidized bed column which is inconvenient and costly once the design of the unit operation is established.

Table 3-1 Liquid-solid mass transfer orrelations :

Reference	Expt. technique	Fluid	Particles	Bed	ε range	Re range	Correlation
Fan et al. (1960)	Dissolution	Water	Granules 7-2.1 mm	Fixed and fluidized bed	0.65-0.9	1020-1520	$Sh = 2 + 1.51(Re(1-\varepsilon))^{0.5} Sc^{(1/3)}$
Couderc et al (1971)	Dissolution	Water	Benzoic acid spheres 4.9-6.1 mm	Fluidized bed	0.5-0.75	100-300	$Sh = \frac{0.0054}{\varepsilon^2} ReSc^{(1/3)}$
Damronglero et al. (1973)	Dissolution	Water	Benzoic acid spheres 4.6-8.2 mm	Fluidized bed	0.6-0.95	1300-1600	$Sh = 0.763\varepsilon^{-1.2} Re^{0.556} (\varepsilon < 0.815)$ $Sh = 0.268\varepsilon^{-2.4} Re^{0.669} (\varepsilon > 0.815)$
Laguerie (1976)	Dissolution	Saturated aqueous soln.	Citric acid crystal	Fluidized bed	0.65-0.95	0.12-1.2	$Sh = 0.36 Re^{0.5} Sc^{0.333} \varepsilon^{-1.8}$

Table 3-1 Cont.

Ref.	Expt. Technique	Fluid	Particles	Bed	ε Range	Re Range	Correlation	Notes
Nanda et al. (1975)	Dissolution	Water	Benzoic acid	Fluidized bed	0.4-0.95	6.5-900	$J_d\varepsilon = .0213f$ $Re'' < 1000$	$J_d = \frac{k}{u}Sc^{(2/3)}$ $Re'' = \frac{d_p u\rho}{\mu(1-\varepsilon)}$ $f = \frac{\nabla\rho g}{\rho u^2}\frac{d_p}{L}\frac{\varepsilon^3}{1-\varepsilon}$
Upadhya and Tripatbi (1975)	Dissolution	Water	Benzoic acid cylinders and pellets	Fluidized bed	0.27-0.91	572-1350	$J_d = 3.8155Re''^{-0.7313}\ (Re'' < 20)$ $J_d = 1.6218Re''^{-0.477}\ (Re'' > 20)$	
Ganho et al (1975).	Adsorption	Phenol in aqueous soln.	Activated carbon	Fluidized bed	0.59-0.83	6-22	$J_d = 2.55Re^{-0.537}$	
Bales et al (1975).	Adsorption	Phenol in aqueous soln.	Activated carbon	Fluidized bed	0.59-0.83	6.5-19.1	$J_d = .044\left[\frac{Re}{(1-\varepsilon)Ga}\right]^{-.527}$	$Ga = \frac{d_p^3\rho(\nabla\rho)g}{u^2}$

It is well known that in a conventional bed, particles are subject to three macroscopic forces : the gravitational force F_g, the drag force F_d, and the buoyancy force F_b. As soon as the drag force, which is measured by the pressure drop ΔP across the bed, balances the other two forces the particles are fluidized.

In MSFB, however, an additional force is created by applying the magnetic field on ferromagnetic particles. The magnetic field magnetizes ferromagnetic particles and creates magnetic forces between the particles. These induced particle-particle forces provide an additional macroscopic force that has to be overcome by the fluid drag force. Hence, the fluid velocity through the bed has to be increased just to compensate this new macroscopic force. The induced particle-particle forces tend to bring the particles together, which results in a decrease of the bed porosity.

Consequently, in MSFB we are able to increase the fluid velocity and at the same time, maintain low bed porosity. This means that the relative velocity between the fluid and the particles is substantially increased; hence, the mass transfer coefficient between the fluidizing particles and the fluid has to increase too.

The previous discussion is illustrated in Figure 3-1.

Figure 3-1 : Illustration of the increase of fluid interstitial velocity in MSFB.

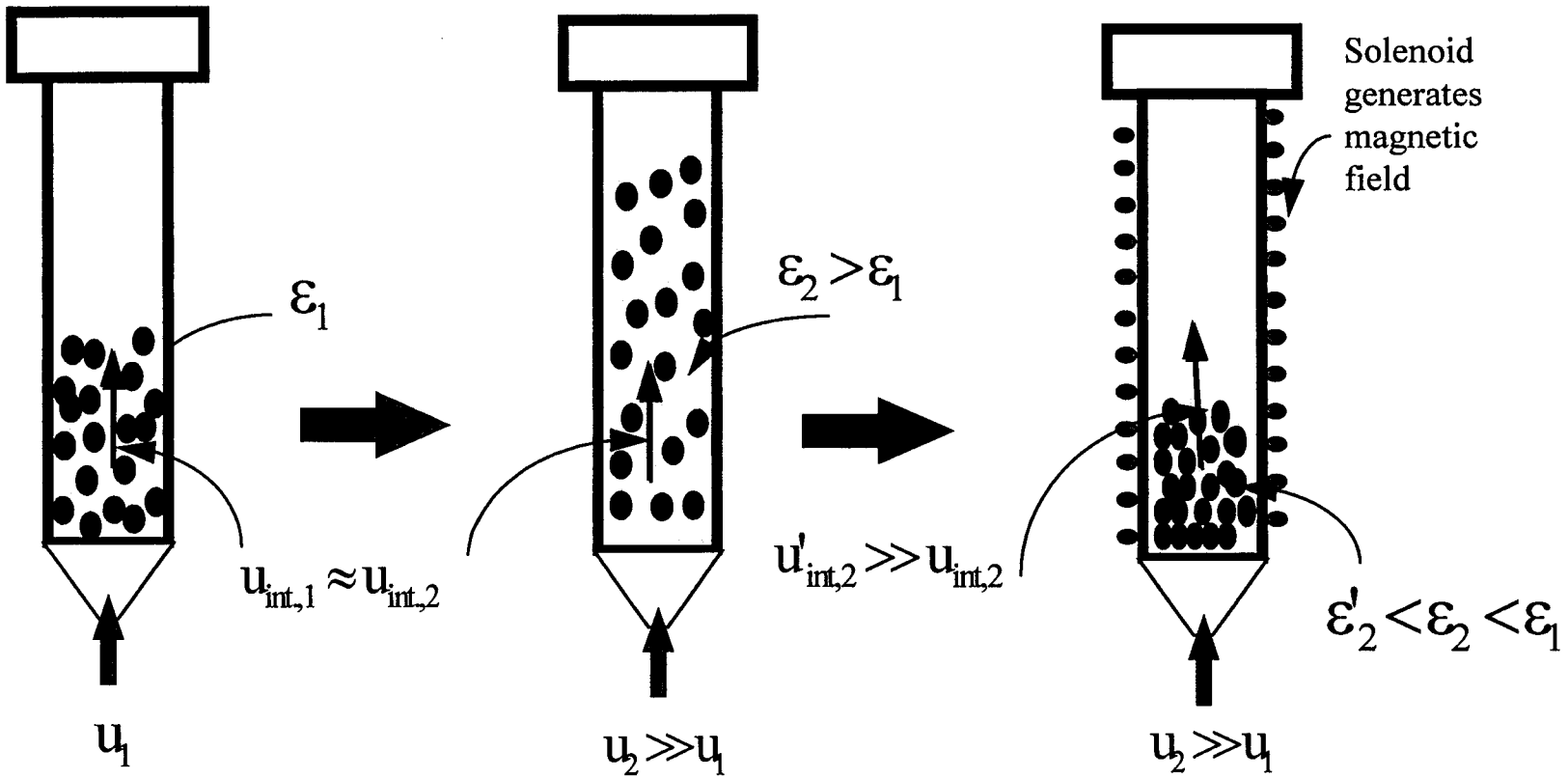

3.2 Mathematical Model for the Adsorption in MSFB.

There are two feasible models that can be used in this study to evaluate mass transfer coefficient in MSFB.

Model (1) : This model presumes that our experimental system is schematically represented by Figure 3-2 :

System boundary(1) represents the part of our system (including part of the fluidization column, overflow box, connecting pipes, pump, rotameter, etc.) where only the adsorbate solution is present (no fluidizing particles). It is assumed that in this volume the fluid is very well mixed and hence the adsorbate concentration C is uniform. System Boundary (2) is the part of our system where the fluidizing particles are in contact with the adsorbate and where the actual mass transfer is taking place.

3.2.1 Model Assumptions : This model assumes that :

1- The adsorbate concentration within system boundary(1), C, is uniform. This is an obvious assumption because no adsorption is taking place there and the recirculating pump is a part of this system.

2- The adsorbate concentration at the inlet of the fluidized bed, C, is not changing substantially while the fluid passes through the fluidized bed - quasi-steady state assumption. This assumption was also used by other investigators, Tang(1990), in the development of models for short bed heights. The maximum bed height that is reached in our experiments is 61 cm with a fluid superficial velocity of 5.7 [cm/s] and a bed

Figure 3-2 : Schematic representation for model(1)

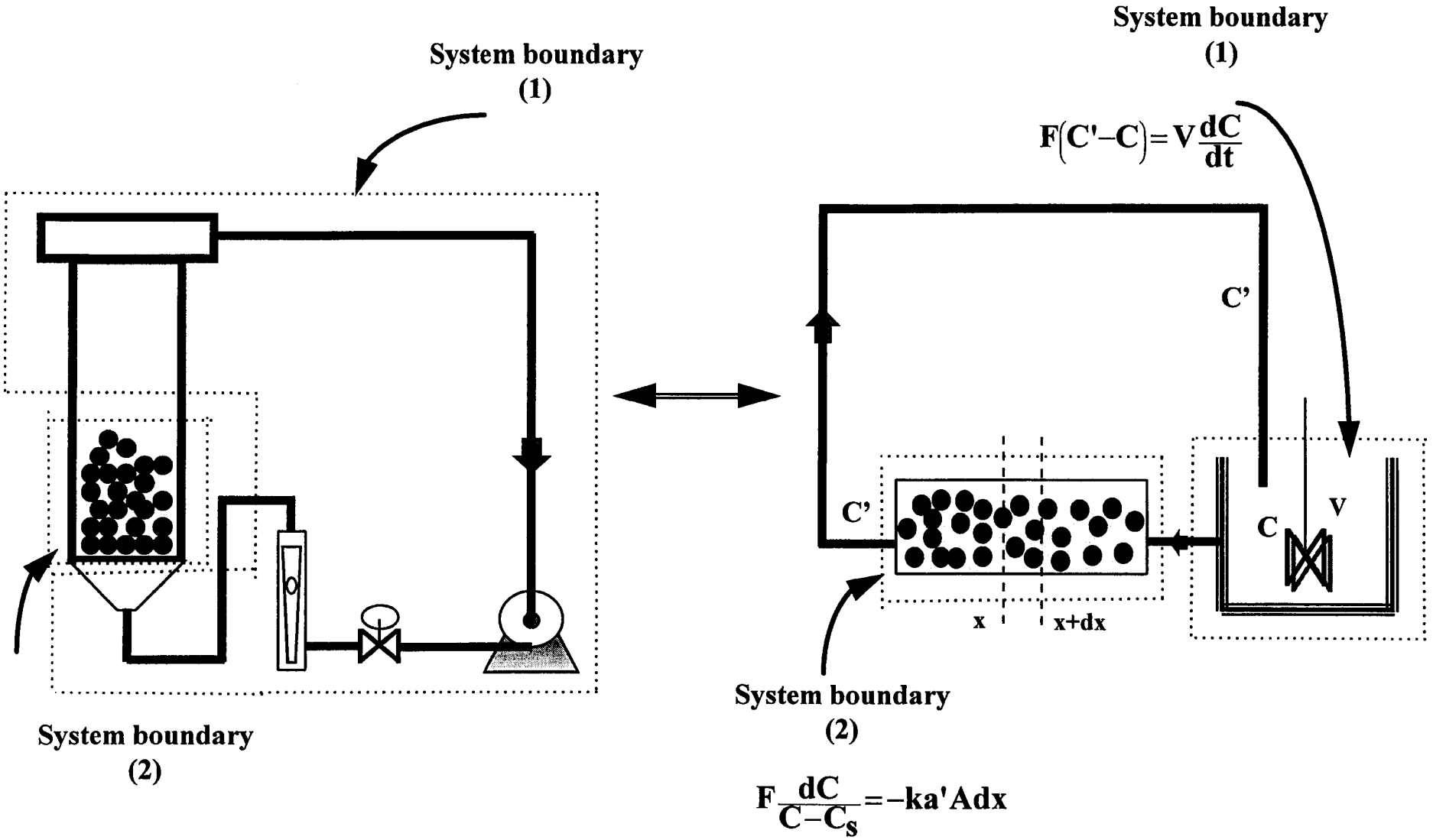

porosity of 0.87. Therefore, it takes a maximum of 9.3 seconds for an element of fluid to pass once through the bed. This represents, however, the worst case scenario in our experiments.

3- The fluid flows in plug flow through the fluidized bed.

4- The adsorbate equilibrium concentration above the particle surface, C_s, is constant during one pass of the fluid through the fluidized bed. This assumption is partially justified by previous assumptions. Besides, as will be explained in Chapter 5, the calculation of the mass transfer coefficient, k, is determined from the initial adsorption data in which C_s does not play substantial role. In fact, if the mathematical model is simplified, as explained below, a rough estimate of mass transfer coefficient could be obtained by even neglecting C_s.

5- The interparticle diffusion resistance is negligible. The fluidizing particles are only made of 2% alginate and 20% ferromagnetic powder by weight which is all together only about 10% by volume. The rest of particle volume is water. Therefore, their internal volume is readily accessible to the adsorbate. Also, as mentioned above, our mass transfer calculation is based on the initial adsorption data, first few seconds, where diffusion resistance plays very minor role. Several investigators, Furusawa and Smith (1973), Mckay (1983), and Silem et al (1993), neglected the interparticle diffusion in the development of their model.

6- The adsorption isotherm is linear. This assumption is also proposed by several researchers, Mckay et al (1985), and Tang (1990). To verify this assumption, the adsorption isotherm is established for this study (see Chapter 4 for details). A linear isotherm is obtained according to the equation :

$$N = K_e C_s$$

3.2.2 Material Balance : System boundary (1)

$$FC' - FC = V\frac{dC}{dt} \quad \Rightarrow \quad F(C'-C) = V\frac{dC}{dt} \qquad (3\text{-}1)$$

For the System Boundary (2) (including quasi-steady state assumption) :

$$(FC)_x - (FC)_{x+\Delta x} - k(C - C_s)da = 0$$

where $a = a'V$ and a' is the area of particles per volume of column . Therefore,

$$F\left(C_{x+\Delta x} - C_x\right) = -k(C - C_s)a'A\Delta x \qquad (3\text{-}2)$$

From equation (3-2), take Lim $\Delta x \rightarrow 0$:

$$F\frac{dC}{dx} = -ka'A(C - C_s)$$

This leads to :

$$F\frac{dC}{C-C_s} = -ka'Adx \tag{3-3}$$

By taking a differential balance of the adsorbate within the particle, we obtain

$$D\left(\frac{\partial^2 C_r}{\partial r^2} + \frac{2}{r}\frac{\partial C_r}{\partial r}\right) - m\frac{\partial N_r}{\partial t} = \frac{\partial C_r}{\partial t} \tag{3-4}$$

also, the overall adsorbate concentration change withen the system is represented by :

$$\frac{dC}{dt} = -ka'(C-C_s) \tag{3-5}$$

Equation 3-5 is exclusively used to find the relation between C and C_s. We assumed that the total amount of MB that disappeared from the solution is all adsorbed onto the particles.

The boundary conditions that are used in solving the above equations are :

$$D\left(\frac{\partial C_r}{\partial r}\right) = k(C-C_s) \tag{3-6}$$

$$\left(\frac{\partial C_r}{\partial r}\right)_{r=0} = 0 \tag{3-7}$$

$$C_r\big|_{t=0} = 0 \tag{3-8}$$

Also, the following boundary conditions are applicable to the previous equations :

BC1	$C=C_0$	$C_s=0$
	$C=C$	$C_s=C_s$

BC2	x=0	C=C
	x=L	C=C'
BC3	t=0	$C=C_0$
	t=t	C=C

Equations 3-1, 3-3, 3-4, and 3-5 along with the above mentioned boundary conditions represent our mathematical model. The model has to be solved numerically. However, the model can be solved analytically if we incorporate the assumptions proposed previously.

By neglecting the interparticle diffusion resistance, as explained in assumption (5), we have the following consequences :

$$C_r = C_s \tag{3-9}$$

$$N_r \text{ is uniform and } N_r = N \tag{3-10}$$

and with the linear isotherm,

$$\frac{dN}{dt} = K_e \frac{dC_s}{dt} \tag{3-11}$$

From equations (3- 4,5,6,7,and 8) we can obtain :

$$m\frac{dN}{dt} = ka(C - C_s) \tag{3-12}$$

Combining equations(3- 11 and 12) we obtain :

$$\frac{dC_s}{dt} = \frac{ka'}{mK_e}(C - C_s) \qquad (3\text{-}13)$$

By dividing equation (3-5) by (3-13), we obtain :

$$\frac{dC}{dC_s} = -mK_e \qquad (3\text{-}14)$$

Equation 3-14 is solved by using boundary condition 1 (BC1), equation 3-3 is solved using BC2, and equation 3-1 is solved using BC3.

The detailed analytical solution to the above model is shown in Appendix F. Useful form of the solution is represented by the following equation :

$$\mathrm{Ln}\left\{\frac{C(1+mK_e)-C_0}{C_0(1+mK_e)-C_0}\right\} = \frac{1+mK_e}{mK_e}\frac{F}{V}\left(e^{-\alpha k}-1\right)t \qquad (3\text{-}15)$$

where $\alpha = \dfrac{a'AL}{F} = \dfrac{a'V}{F}$

Model (2) : This model assumes that the particles and the adsorbate are in contact with each other throughout the whole volume of the system as if our system is a well mixed agitated tank (see Figure 3-3). This model can be represented by the same equations and boundary conditions as those of model (1) excluding equations (3-1,2 and 3) and BC2.

Figure 3-3 :Schematic representation for model(2)

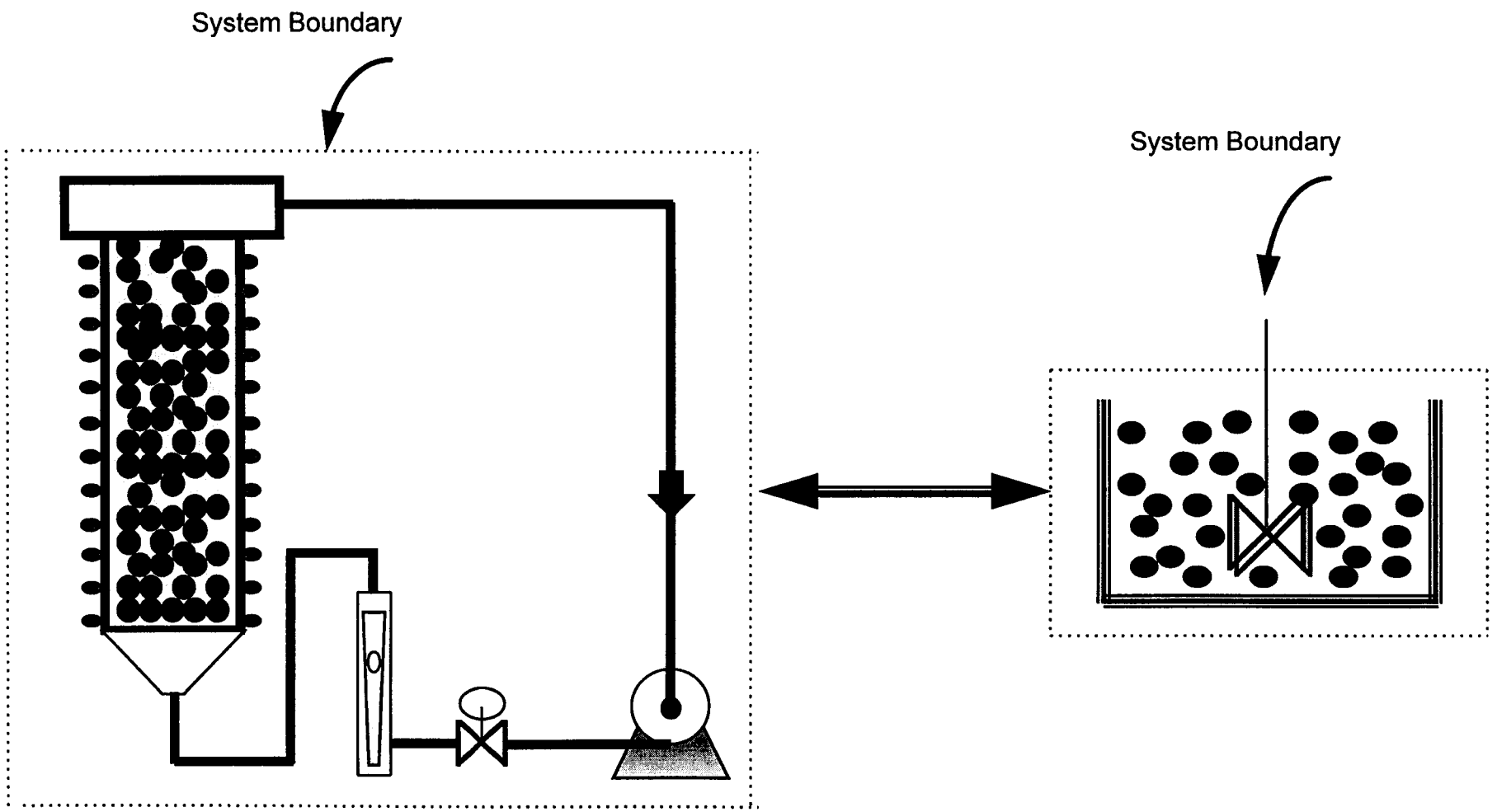

The detailed analytical solution is shown in Appendix G. Useful form of the solution of this model is represented by the following equation :

$$\mathrm{Ln}\left\{\frac{C(1+mK_e)-C_0}{C_0(1+mK_e)-C_0}\right\}=-\frac{1+mK_e}{mK_e}(ka')t \qquad (3\text{-}16)$$

Model(1) and model(2) can be simplified even further if we incorporate the assumption that C_s is zero at the very beginning of the adsorption experiment when we may decide to determine the slope of the C-t curve. In this case the solution of the model(1) is simplified and reduced to the following equation :

$$\mathrm{Ln}\left(\frac{C}{C_0}\right)=\frac{F}{V}\left(e^{-\alpha k}-1\right)t \qquad (3\text{-}17)$$

and the solution to the model(2) is simplified to the following equation :

$$\mathrm{Ln}\left(\frac{C}{C_0}\right)=-ka't \qquad (3\text{-}18)$$

Those simplifications, which can be used to anticipate rough values for the mass transfer coefficient, are shown in detail in Appendix H.

Model(2) has been used to measure liquid-particle mass transfer coefficient in well agitated vessels by several investigators, Furusawa and Smith (1973), and McKay (1983). We can also use this model for our system if we neglect the volume of liquid outside the fluidized bed or if we have a very high liquid inlet velocity. In other words, model(1) can be reduced to model(2) only if V is too small or if F is too large. If any of the previous conditions is satisfied, $e^{-\alpha k}$ term in equation 3-15 is reduced to $(1-\alpha k)$. This will simplify equation 3-15 to equation 3-16.

However, the liquid volume outside the fluidized bed contributes substantially to the overall liquid volume of our experimental system. Besides, our liquid circulating pump capacity and the height of our fluidizing column do not allow us to operate at very high liquid velocities. Therefore, the use of the model(2) for the evaluation of the mass transfer coefficient could yield unrealistic results. Hence, model(1) is much more realistic representation of our experimental system and it will be used in this study to evaluate liquid-solid mass transfer coefficient.

CHAPTER 4
EXPERIMENTAL MEASUREMENTS

4.1 Adsorption Isotherm

As explained in the section 3-2, a linear relationship is assumed between equilibrium concentration of methylene blue (MB) in the solution and the amount of MB adsorbed on the particles. To verify this assumption, the adsorption isotherm for MB and the fluidizing particles is determined by measuring the steady state equilibrium MB concentration in the solution, C_s for different initial concentrations C_0. The steady state equilibrium MB concentration is measured by recording the MB UV absorbance, which is a linear function of the MB concentration, at different time intervals for about three hours, as shown in Figure 4-1. The point at which the MB absorbance no longer changes with time corresponds to the steady state MB concentration. In every run the same amount of particles are used. Then, a plot of C_s versus N is established, where N is the concentration of MB adsorbed on the fluidizing particles and it is evaluated from the equation :

$$N = \frac{C_0 - C_s}{m} \qquad (4\text{-}1)$$

where m is the amount of particles used per unit volume of fluid.

Figure 4-1 : Steady state MB equilibrium concentration measurements

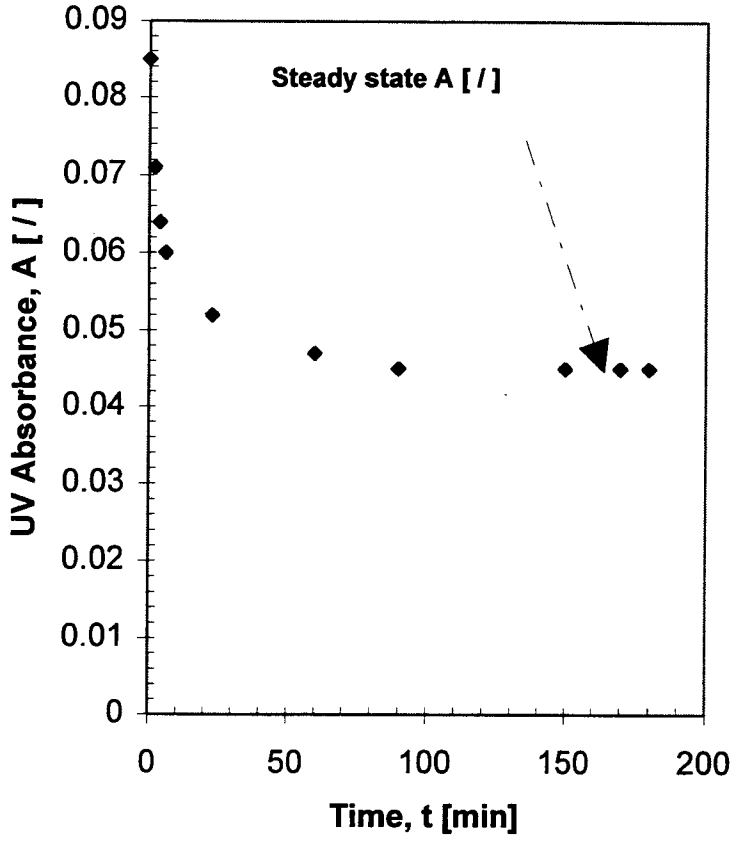

Table 4-1 reports our adsorption isotherm data. The isotherm so obtained at 25^0C is shown in Figure 4-2.

In our experiments, MB initial absorbance does not exceed 0.2 [%]. This corresponds to an initial concentration C_0 of less than 0.06 [mg/ml]. In this initial concentration range, the adsorption isotherm shows a noticeable linear relationship between C_s and

N. These low concentration data are plotted in Figure 4-3. The data are linearly fitted and the following relationship is obtained :

$$N = K_e C_s \tag{4-2}$$

where K_e is the adsorption equilibrium constant and its value is the slope of the fitted straight line.

Table 4- 1 : Adsorption isotherm data

C_0[mg/ml]	N [mg of MB./g Of particles]	Steady state MB conc.,Cs[mg/ml]
0.017	0.237	0.005
0.0256	0.405	0.006
0.042	0.644	0.011
0.064	1.025	0.014
0.090	1.494	0.018
0.117	2.011	0.019
0.141	2.517	0.020
0.170	3.052	0.022

Figure 4- 2 : Adsorption isotherm plot

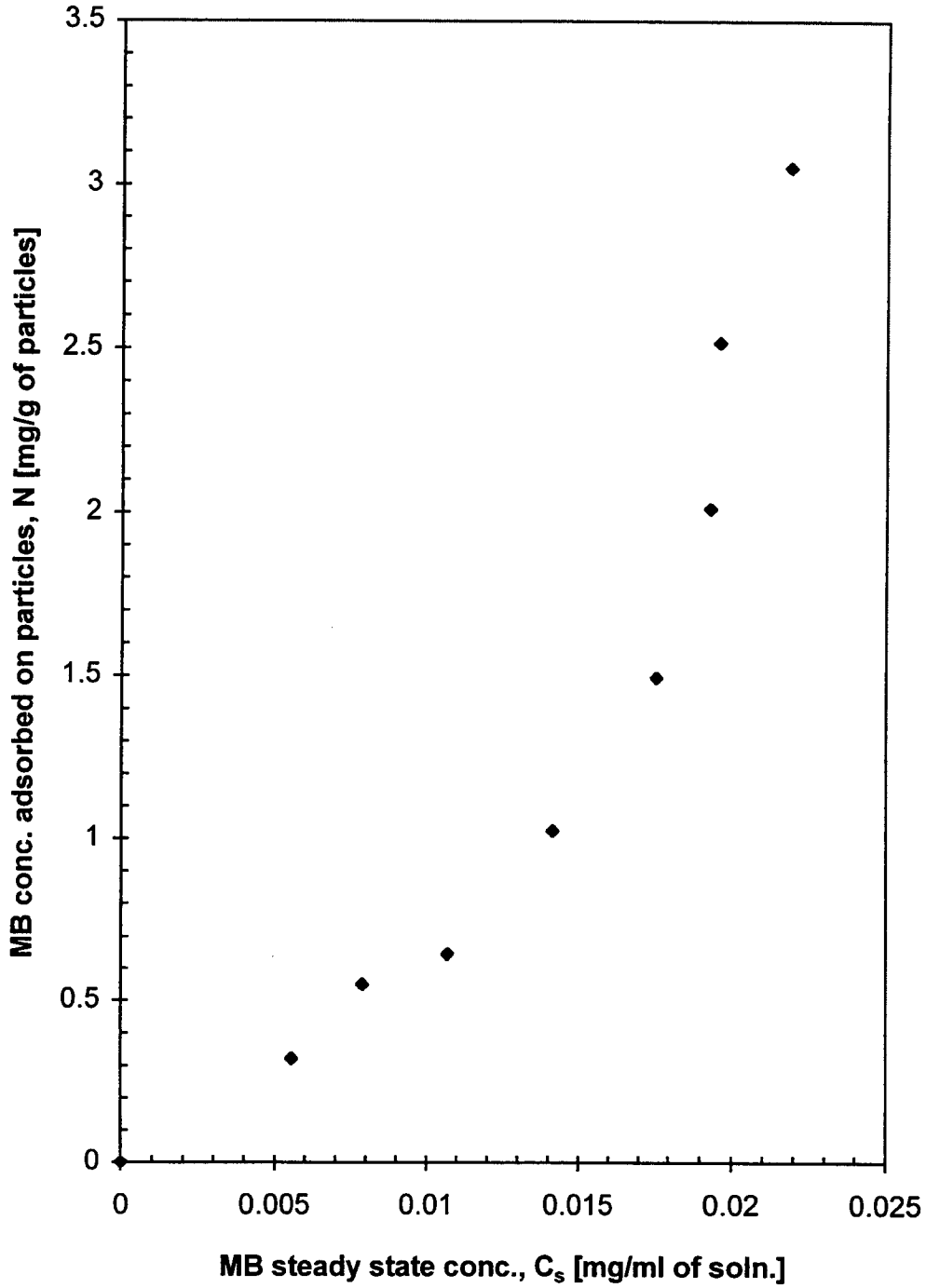

Figure 4- 3 : Linear adsorption isotherm for low MB. conc.

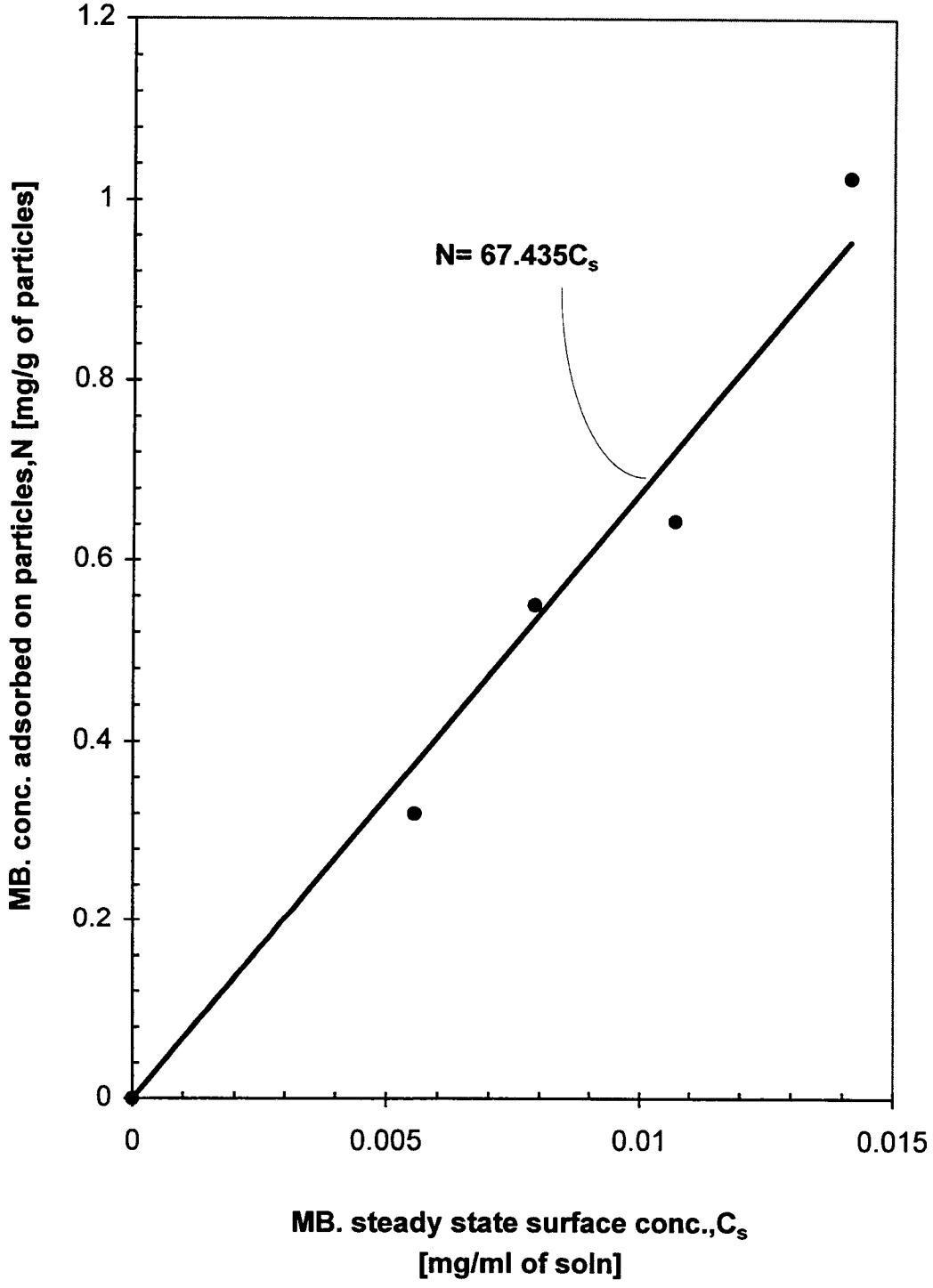

4.2 The Height and Porosity of the Bed

The pressure drop, ΔP_i, between the top of the bed, P_t, and any other level at pressure port, P_i, can be easily calculated

$$\Delta P_i = P_i - P_t \tag{4-3}$$

We can determine the bed height, L, by plotting ΔP_i against the corresponding height of the ith pressure port, L_i. Figure 4-3 presents this plot. It is clear that ΔP_i is linearly decreasing as L_i increases until it becomes zero. Hence, the first value of L_i that corresponds to a $\Delta P_i = 0$ is the height of the bed L.

For a uniform bed viodage, ε, a simple force balance across the fluidized bed is given by :

$$\Delta P = \Delta L(\rho_p - \rho)(1-\varepsilon)g \;\Rightarrow\; \frac{\Delta P}{\Delta L} = [\rho_p - \rho]g[1-\varepsilon] \tag{4-5}$$

where $\frac{\Delta P}{\Delta L}$ is the inverse of the slope of the straight line obtained from Figure 4-4.

Hence, the bed porosity (viodage) ε is evaluated as :

$$\varepsilon = 1 - \frac{\Delta P}{\Delta L[\rho_p - \rho]g} \tag{4-6}$$

Figure 4-4 : Bed height measurement for uniform bed porosity

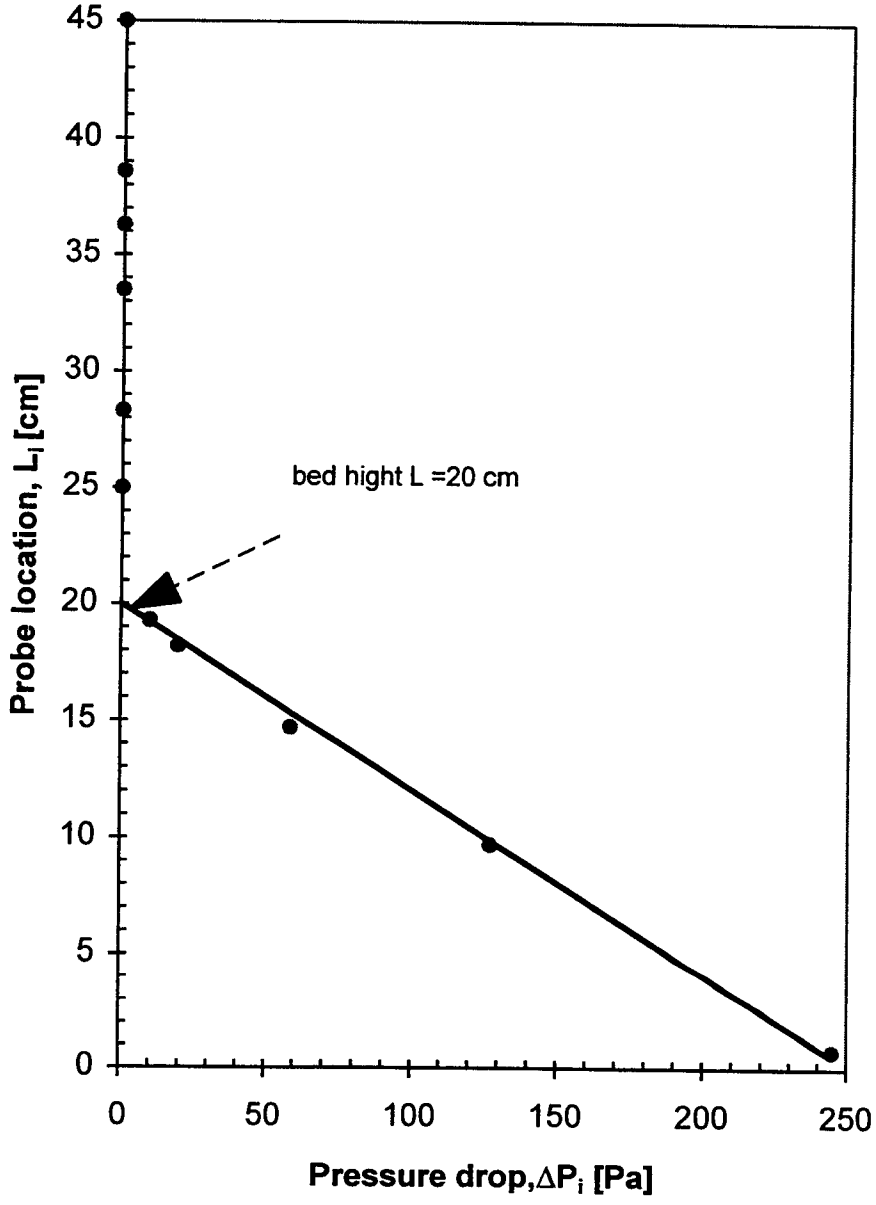

Also, the bed porosity can be evaluated using a simple particle material balance equation

$$\rho A L_0 (1-\varepsilon_0) = \rho A L (1-\varepsilon) \tag{4-7}$$

which leads to :

$$\varepsilon = 1 - \frac{L_0(1-\varepsilon_0)}{L} \tag{4-8}$$

where L_0 and ε_0 are our packed bed height and porosity respectively.

Equation 4-6 is appropriate only for a fluidized bed with uniform porosity. However, It is well known that the fluidized bed porosity is not uniform, Kunii and Levenspel (1991), especially not for higher fluid superficial velocities u_0. The bed viodage is low and uniform in the lower portion of the bed, and becomes lean and non uniform toward the top of the bed, Honorez(1994).

In our experiments, for the superficial velocities $u_0 > 3.7$ [cm/s], we can easily distinguish two zones of the fluidized bed which have two different bed porosities. This has been observed visually and confirmed from the ΔP_i versus L_i plots. In these cases, a mass average bed porosity is evaluated by the following equation :

$$\varepsilon_{avg.} = \frac{\Delta L_1}{L}\varepsilon_1 + \frac{\Delta L_2}{L}\varepsilon_2 \tag{4-9}$$

where ΔL_1 and ΔL_2 are the heights of the dense and lean zones of the bed. Figure 4-5 shows clearly the existence of two different fluidization / viodage zones.

Viodages ε_1 and ε_2 are evaluated from the balance of forces in the two fluidization zones, similar to equation 4-5, which leads to the following equations :

$$\varepsilon_1 = 1 - \frac{\Delta P_1}{\Delta L_1 [\rho_p - \rho] g} \tag{4-10}$$

$$\varepsilon_2 = 1 - \frac{\Delta P_2}{\Delta L_2 [\rho_p - \rho] g} \tag{4-11}$$

where $\frac{\Delta P_1}{\Delta L_1}$ and $\frac{\Delta P_2}{\Delta L_2}$ are the inverse of the slopes of the two fitted straight lines shown in Figure 4-5.

To confirm the bed height measurements, Visual bed height observations are also recorded. Hence, bed porosity is evaluated simply by using equation 4-8.

Figure 4-5 : Determination of the bed height, L, for a non uniform bed porosity

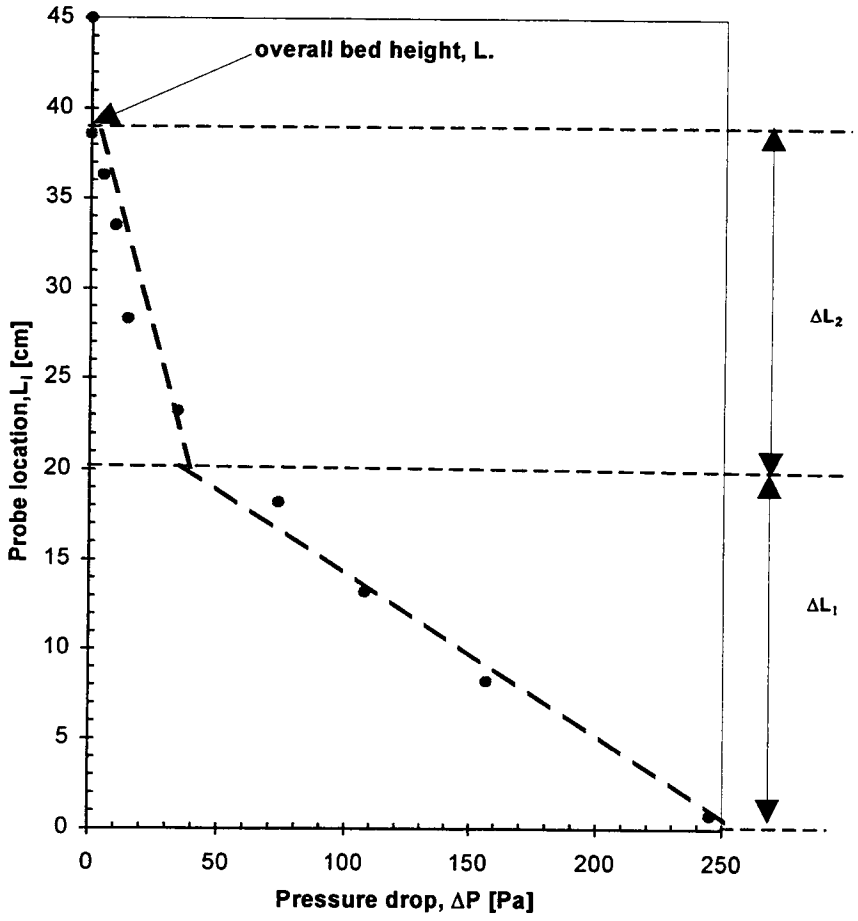

Visual observations, along with porosities calculated from equation 4-8, are very close to our experimental measurements, with a maximum error of 3.09 %. Experimental

and visual observations of the bed heights and porosities for different fluid velocities and different magnetic field intensities are tabulated in Table 4-2.

4.3 Measurements of the MB Concentration in the Magnetically Stabilized Fluidized Bed MSFB.

Original concentration data using the MB adsorption on the fluidizing particles are reported in Appendix I. Different fluid superficial velocities and different magnetic field intensities are used. In all experiments, the same amount of the fluidizing particles and fluid volume are maintained.

Table 4-2 : Bed height and porosity measurements for different fluid velocities and magnetic field intensities

u [cm/s]	H [A/m]	$\Delta P_1/\Delta L_1$[Pa/cm]	$\Delta P_2/\Delta L_2$[Pa/cm]	ε_1[/]	ε_2[/]	ΔL_1[cm]	ΔL_2[cm]	L[cm]	$\varepsilon_{avg.}$(/)	$L_{obs.}$[cm]	$\varepsilon_{obs.}$(/)
3.2	0	0.115	-	0.69	-	25.0	0.0	25	0.69	25	0.70
3.2	7930	0.138	-	0.63	-	20.0	0.0	20	0.63	20	0.63
3.2	12886	0.139	-	0.62	-	19.0	0.0	19	0.62	19	0.61
3.7	0	0.113	0.034	0.69	0.91	22.5	13.4	36	0.77	36	0.79
3.7	3965	0.094	-	0.75	-	32.0	0.0	32	0.75	32	0.77
3.7	7930	0.105	-	0.72	-	27.0	0.0	27	0.72	27	0.72
3.7	12886	0.127	-	0.66	-	22.0	0.0	22	0.66	-	-
4.5	0	0.097	0.017	0.74	0.95	26.2	18.7	45	0.83	45	0.83
4.5	4956	0.099	0.022	0.73	0.94	25.1	10.8	36	0.80	36	0.79
4.5	7930	0.116	0.034	0.69	0.91	22.1	9.8	32	0.76	32	0.77
4.5	9912	0.123	0.037	0.67	0.90	20.5	6.5	27	0.72	27	0.72
4.5	12886	0.114	-	0.69	-	24.0	0.0	24	0.69	24	0.69

Table 4-2 cont.

u [cm/s]	H [A/m]	$\Delta P_1/\Delta L_1$[Pa/cm]	$\Delta P_2/\Delta L_2$[Pa/cm]	ε_1[/]	ε_2[/]	ΔL_1[cm]	ΔL_2[cm]	L[cm]	$\varepsilon_{avg.}$(/)	$L_{obs.}$[cm]	$\varepsilon_{obs.}$(/)
5.2	0	0.085	0.013	0.77	0.96	29.4	31.6	61	0.87	61	0.88
5.2	5947	0.102	0.016	0.73	0.96	25.2	18.8	44	0.82	44	0.83
5.2	7930	0.108	0.016	0.71	0.96	23.5	12.4	36	0.79	36	0.79
5.2	9912	0.115	0.015	0.69	0.96	22.1	9.9	32	0.77	32	0.77
5.2	12886	0.109	-	0.71	-	27.0	0.0	27	0.71	27	0.72
5.2	14868	0.107	-	0.71	-	25.0	0.0	25	0.71	25	0.70
5.7	5947	0.092	0.023	0.75	0.94	28.2	32.8	61	0.85	61	0.88
5.7	7930	0.094	0.020	0.75	0.95	27.0	18.0	45	0.83	45	0.83
5.7	9912	0.112	0.015	0.70	0.96	22.7	13.4	36	0.80	36	0.79
5.7	12886	0.122	0.015	0.67	0.96	20.9	11.1	32	0.77	32	0.77
5.7	16850	0.116	-	0.69	-	23.2	-	23	0.69	23	0.67

CHAPTER 5
Experimental Results And Discussion

The mathematical model (developed in Chapter 3), which describes our experimental system, clearly shows that we need reliable information about the average bed porosity before we can evaluate the fluid-particle mass transfer coefficients from the collected data.

The experiments conducted in this study and previous work done by Jovanovic et al. (1993), and Honorez (1994), enable us to determine the relationship which describes the average bed porosity as a function of magnetic field intensity and fluid superficial velocity.

5-1 The Average Bed Porosity

As reported in Chapter 4, bed porosities were experimentally determined for different fluid superficial velocities, and different magnetic field intensities (see Table 4-2). Figure 5-1 shows the average bed porosity as a function of fluid superficial velocity for different magnetic field intensities. Figure 5-2 shows the average bed porosity as a function magnetic field intensity for different fluid superficial velocities. From these Figures, within the range of experimental conditions, we can conclude that:

1- for a given magnetic field intensity, the average bed porosity increases as fluid superficial velocity increases, and

Figure 5- 1 : The average bed porosity as a function of superficial fluid velocity for different magnetic field intensities.

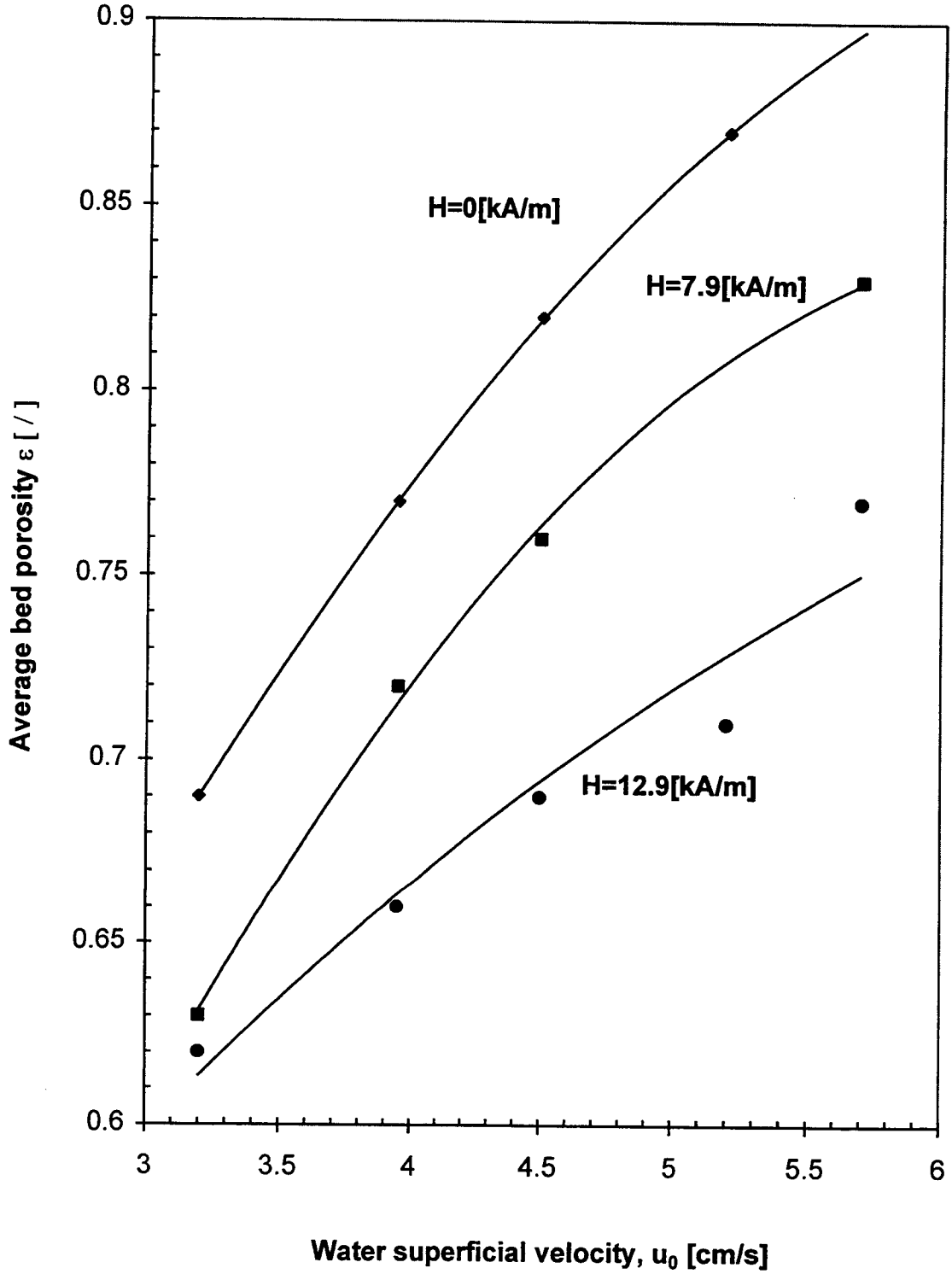

Figure 5- 2 : The average bed porosity as a function of magnetic field intensity for different superficial velocities

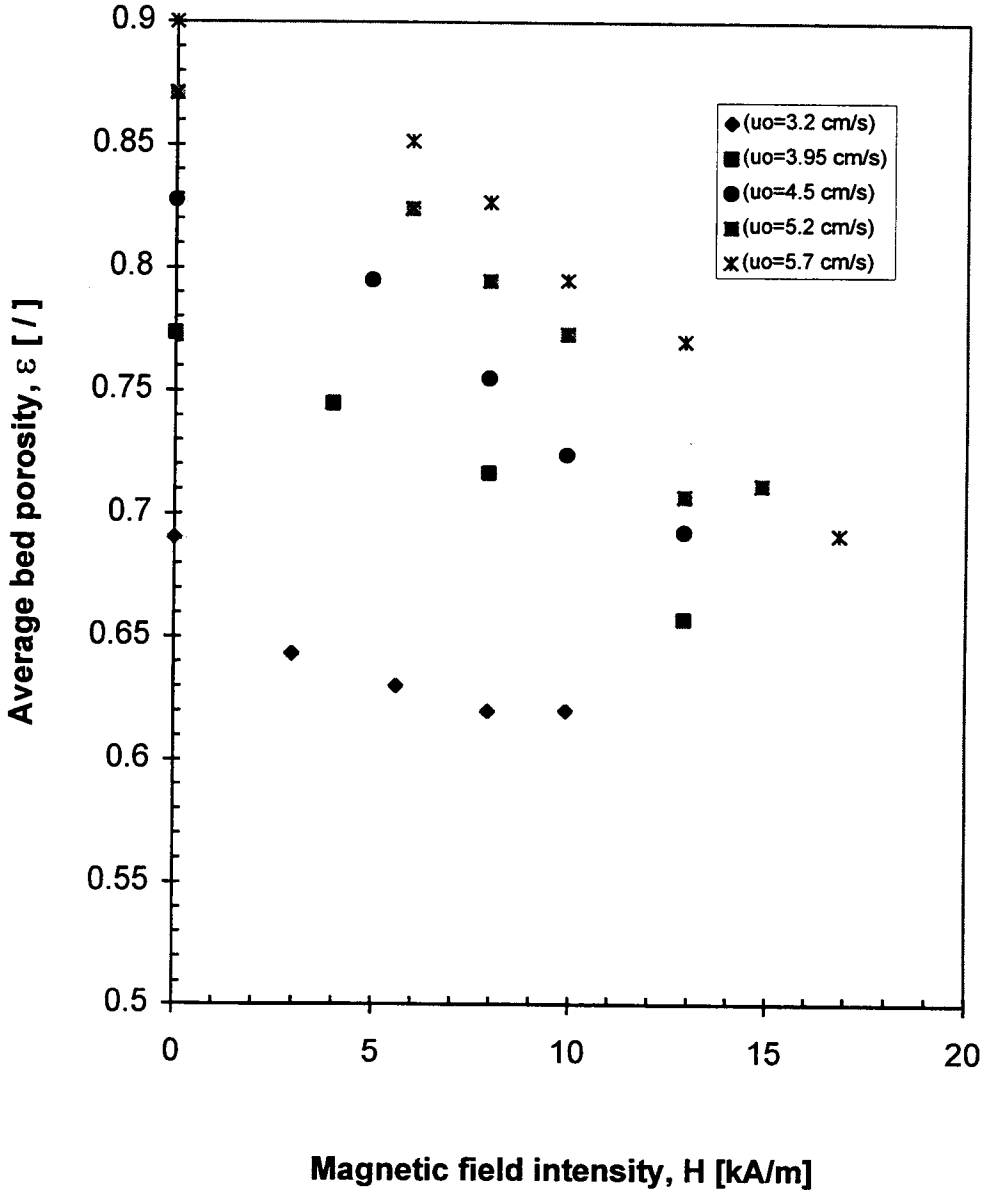

2- for a given fluid superficial velocity, the average bed porosity decreases as magnetic field intensity increases.

This is in agreement with previous studies in liquid-solid fluidization, Siegell (1987), Jovanovic et al.(1993), and Honorez (1994). The figures obtained are analogous to those obtained by Honorez (1994). Hence, we can with confidence use the equation obtained by Honorez (1994) to correlate our data. The equation proposed by Honorez (1994) has the following form,

$$\frac{H_{ms}}{1-\varepsilon}\ln\left(\frac{\varepsilon-\varepsilon_{ms}}{\varepsilon_{ff}-\varepsilon_{ms}}\right)=-(\alpha H^2+\beta H) \quad \Rightarrow$$

$$\varepsilon=\varepsilon_{ms}+(\varepsilon_{ff}-\varepsilon_{ms})\exp\left(-(1-\varepsilon)(\alpha H+\beta)\frac{H}{H_{ms}}\right) \tag{5-1}$$

where ε_{ff} is the porosity of an ordinary fluidized bed (H=0), ε_{ms} and H_{ms} are the bed porosity and magnetic field intensity at the transition between the partially stabilized and stabilized fluidization regime. This characteristic transition is attained when the bed porosity reaches the minimum value and no longer decreases with the increase of the magnetic field intensity, i.e., the ferromagnetic particles are "frozen". The detailed description of this and other fluidization regimes are describe elsewhere, Rosensweig (1981), Casal and Arnaldos (1991), and Honorez (1994). The term ($\alpha H+\beta$) is the magnetic susceptibility χ and it differs for different ferromagnetic

materials. Figure 5-3 shows how experimentally obtained porosities compare with porosities calculated from equation 5.1.

We can now conclude that the magnetic field intensity has significant effect on the bed porosity. This is the result that we expected and which we believe will have the greatest influence on the enhancement of the fluid-solid mass transfer coefficient. Even though the measured bed porosities do not most accurately fit the equation proposed by Honorez (1994), the trend is analogous to that obtained by Honorez (1994). However, by minimizing the sum of the squared differences between the measured and calculated bed porosities, we found that the experimental bed porosities fit equation 5-1 reasonably well when the magnetic susceptibility, χ is changed to the value of , χ= 8.0[/], as shown in Figure 5-4.

5.2 Mass Transfer Coefficient (k) Calculation :

The following parameters are kept constant in all of the experiments conducted in this study :

V_L= 6200 [ml]

M = 300 [g]

K_e= 67.44 [ml of solution / g of particles]

Figure 5-3 : Plot of measured bed porosities against calculated values from equation 5-1

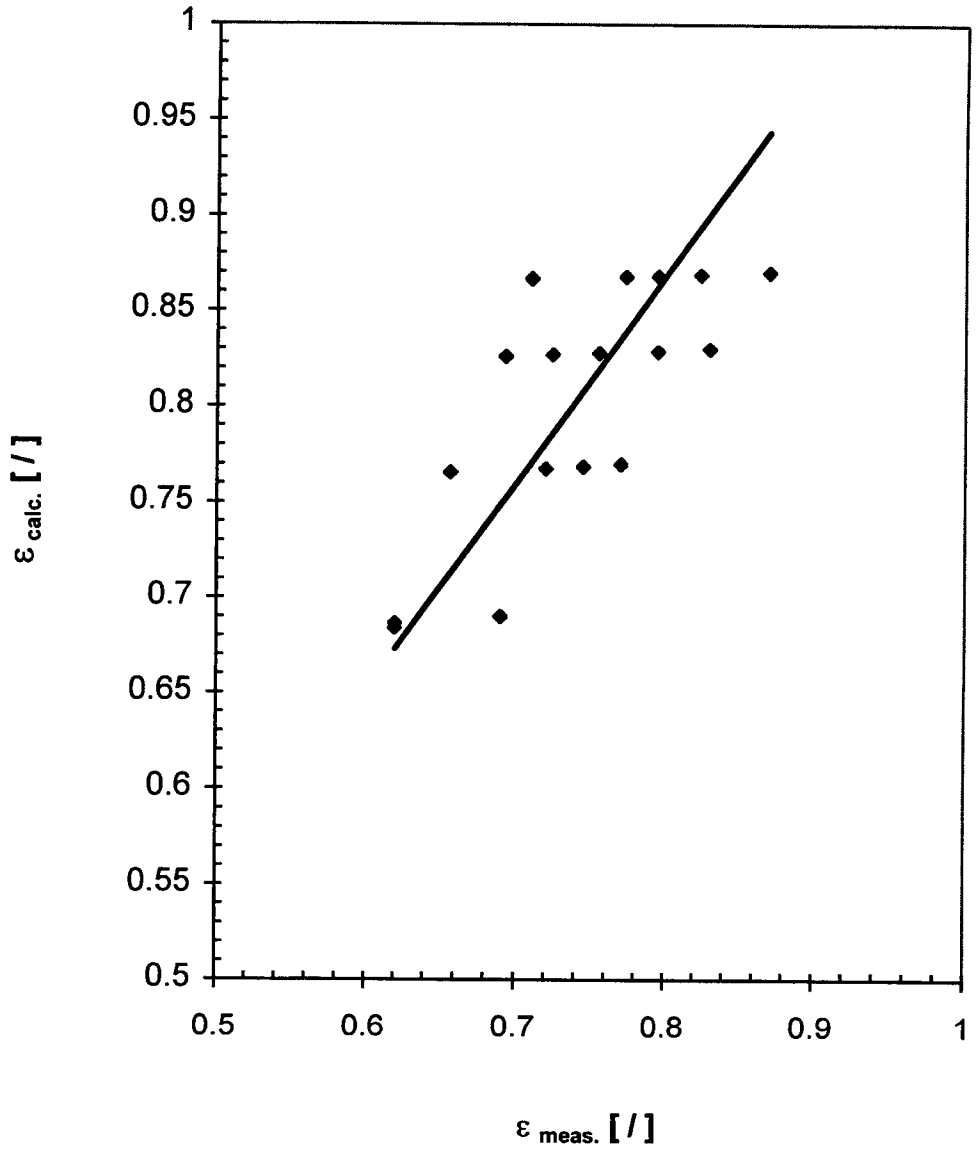

Figure 5-4 : Measured bed porosities against calculated values from equation 5-1, with modified χ

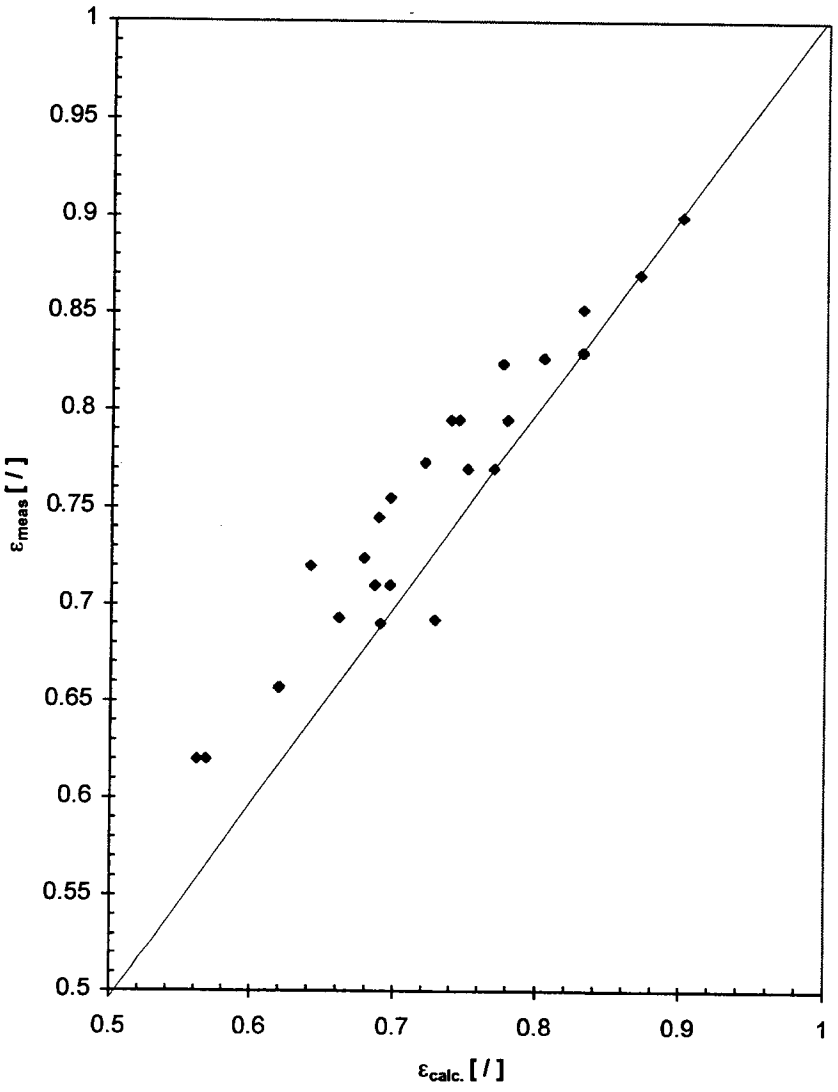

ε_0= **0.375** **[/]**

d_p= **1.5** **[mm]**

L_0= **12** **[cm]**

The calculation of the fluid-solid mass transfer coefficient is based on the outer surface of particles which is calculated as :

$$a' = \frac{(1-\varepsilon)A_p}{V_p} = \frac{6(1-\varepsilon)}{d_p} \tag{5-2}$$

Furthermore equation 3-13 can be written as :

$$\ln\left(\frac{(C/C_0)(1+mK_e)-1}{mK_e}\right) = \frac{1+mK_e}{mK_e}\frac{F}{V}(e^{-\alpha k}-1)t \tag{5-3}$$

Hence, a plot of $\ln\left(\frac{(C/C_0)(1+mK_e)-1}{mK_e}\right)$ versus time, t should give us a straight line with a slope, S,

$$S = \frac{1+mK_e}{mk_e}\frac{F}{V}(e^{-\alpha k}-1) \; . \tag{5-4}$$

However, as shown in Figure 5-5, we see that the plot shows a clear straight line only at the beginning of the adsorption and then it starts to deviate from linearity. Equation 5-3 is developed under the assumption that the mass transfer resistance due to diffusion within the particle is negligible. Obviously, this is not the case and we have to be very careful how to measure the slope of equation 5-3. Consequently, our slope is taken at the beginning of the adsorption data where the plot is clearly linear and our assumption of neglecting diffusion resistance is reasonably valid, primarily due to low equilibrium concentration on the outer particle surface.

Substituting the values of the slopes into equation 5-4, we can obtain :

$$S = 1.3\frac{F}{V}(e^{-\alpha k} - 1) \qquad \Rightarrow \qquad (5\text{-}5)$$

$$k = -(1/\alpha)\ln\left(\frac{SV}{1.3F} + 1\right) \qquad (5\text{-}6)$$

where :

$$F = Au = 30.6\ u \qquad (5\text{-}7)$$

Figure 5-5 : Determination of the slope that is used to calculate mass transfer coefficient, k.

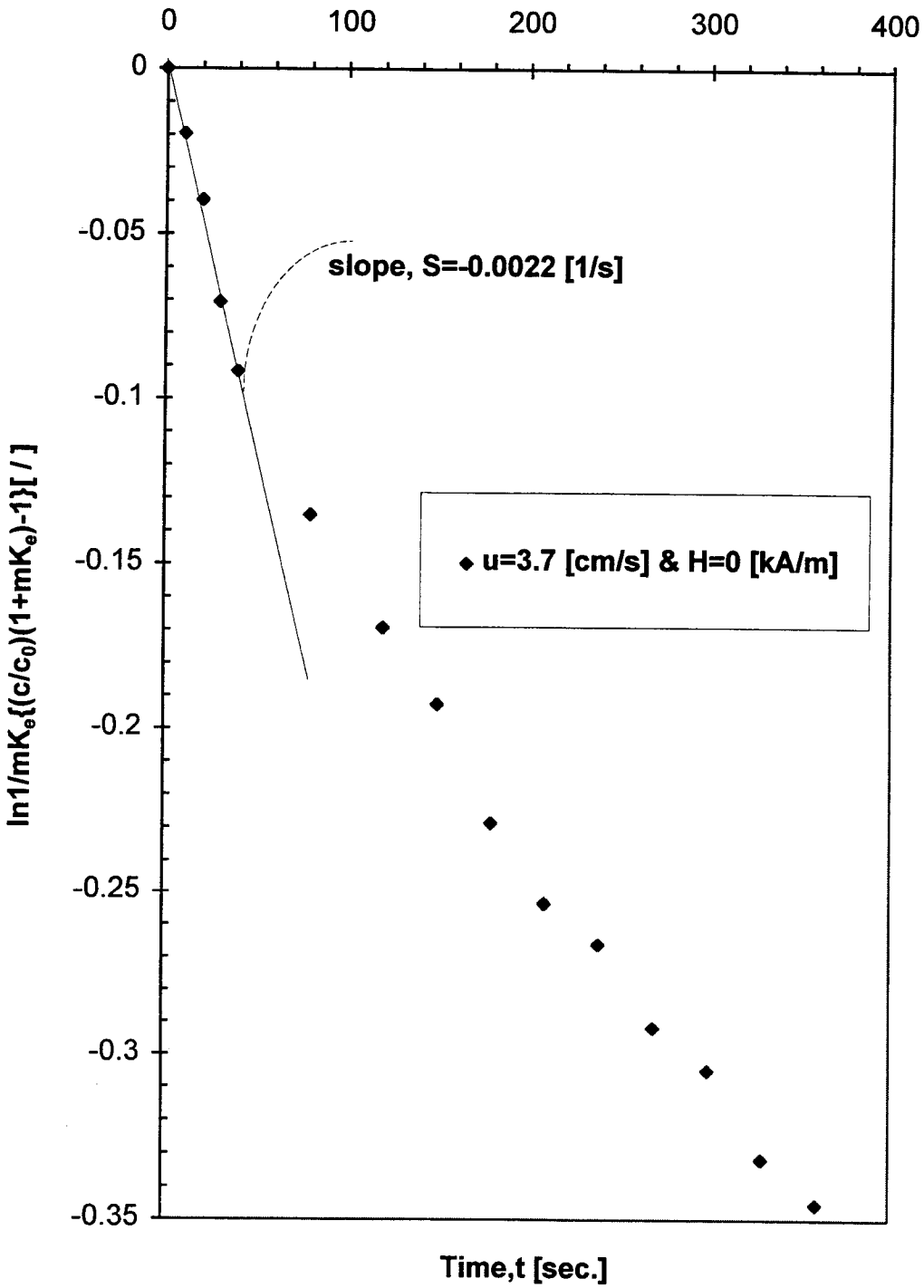

and : $$V = V_L - AL\varepsilon = 6200 - \frac{191.25\varepsilon}{(1-\varepsilon)} \quad (5\text{-}8)$$

L is evaluated by making use of equation 4-10 :

$$L = \frac{L_0(1 \quad \varepsilon_0)}{(1-\varepsilon)} = \frac{7.5}{(1-\varepsilon)} \quad (5\text{-}9)$$

α was defined as :

$$\alpha = \frac{a'AL}{F} = \frac{300}{u} \quad (5\text{-}10)$$

From the above equations, mass transfer coefficient k is evaluated as :

$$k = -(u/300)\ln\left(\frac{S(6200 - \frac{191.25\varepsilon}{1-\varepsilon})}{39.8u} + 1\right) \quad (5\text{-}11)$$

For the particular values shown in figure 5-5, S= -0.022 [1/s], u = 3.7 [cm/s], and ε = 0.765, we can calculate the mass transfer coefficient, k = 0.0011 [cm/s].

Table 5-1 summarizes the values of the measured mass transfer coefficients for different fluid velocities and different magnetic field intensities. Some values of the enhancement of the mass transfer coefficient are plotted as a function of magnetic field intensities for different fluid velocities. The plot is shown in Figure 5-6.

Table 5- 1 :Mass transfer coefficients for different fluid velocities and different magnetic field intensities

u_0 [cm/s]	ε [/]	H [kA/m]	k x 1000 [cm/s]	k enhancement [%]
3.2	0.70	0.00	0.87	0
3.2	0.64	2.97	1.27	46%
3.2	0.62	5.60	1.51	75%
3.7	0.76	0.00	1.10	0
3.7	0.70	5.60	1.30	18%
3.7	0.66	7.53	1.54	40%
4.5	0.83	0.00	1.21	0
4.5	0.79	5.00	1.37	13%
4.5	0.77	7.93	1.50	24%
4.5	0.70	11.89	1.72	42%
4.5	0.69	12.90	1.78	47%
5.7	0.89	0.00	1.30	0
5.7	0.83	7.93	1.64	26%
5.7	0.79	9.90	1.80	38%
5.7	0.77	12.90	2.00	54%

Figure 5-6 : Mass transfer coefficient enhancement as a function of magnetic field intensities for different fluid velocities

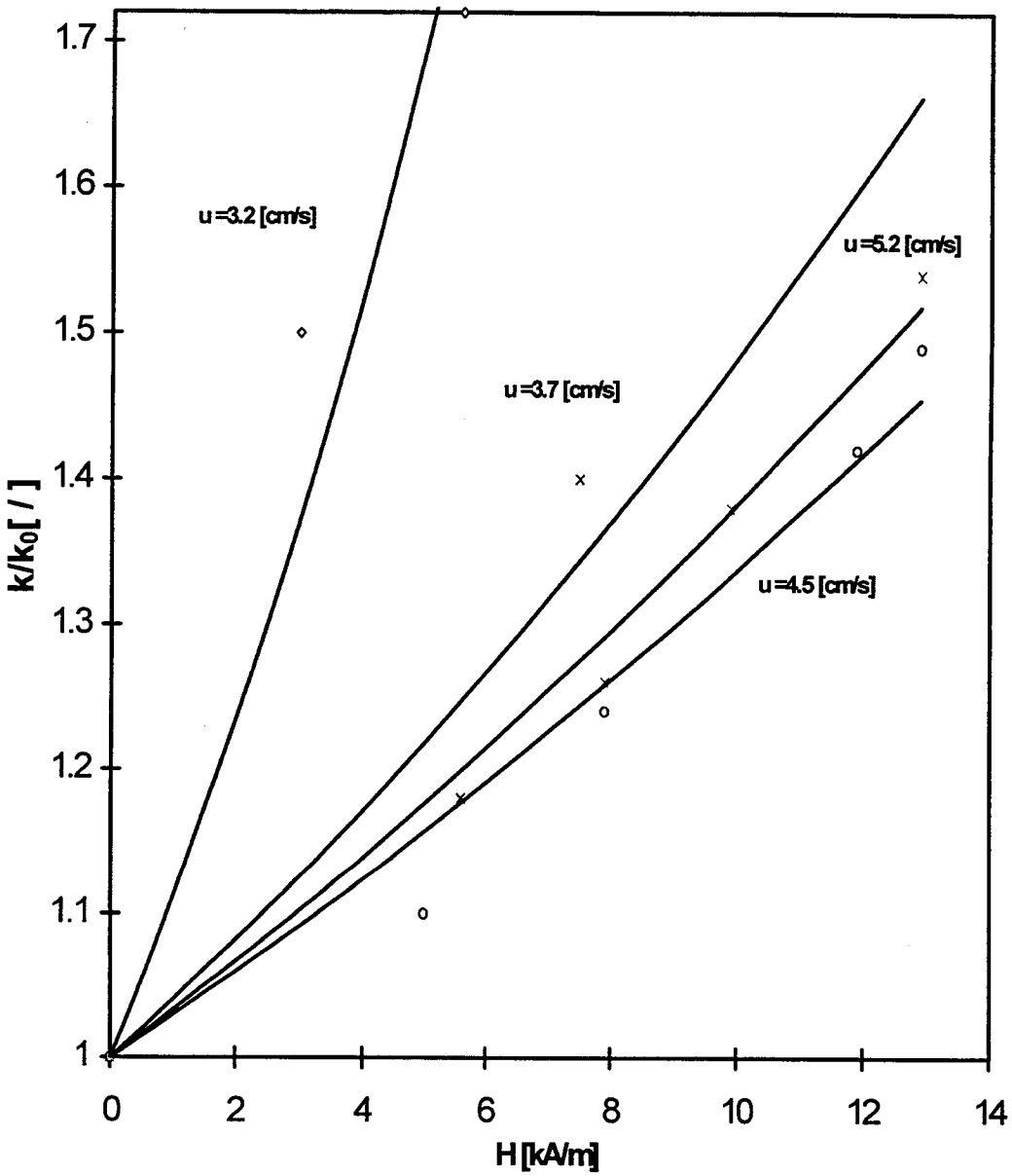

From Table 5-1 and Figure 5-6, we can conclude the following :

- For a given fluid superficial velocity, mass transfer coefficient increases as magnetic field intensity increases. We believe that this is caused by the decrease in the bed porosity. As demonstrated in section 5-1, the average bed porosity decreases with the increase of magnetic field intensity for a given superficial velocity. In fact, this is the result that we anticipated at the beginning of the research. As the bed porosity decreases for a given superficial velocity, the fluid interstitial velocity must increase, which results in a higher fluid-particle relative velocity and hence, a better mass transfer coefficient.

- Still another way of demonstrating the effect of magnetic field intensity on the enhancement of mass transfer coefficient is shown in Figure 5-7. For a given bed height (void fraction), mass transfer coefficient increases as magnetic field intensity increases. This Figure shows that for the same bed height, MB. is adsorbed faster in the bed where higher magnetic field intensity is applied. Hence, a sharper slope, S, and consequently a higher mass transfer coefficient is obtained. Thus, by applying the magnetic field, we are able to maintain the same bed height for higher velocities and hence, a better fluid-particle mass transfer is obtained.

- It is noticed that the increase of mass transfer coefficient for the lowest fluid superficial velocity ($u_0 = 3.2$[cm/s]) is higher than that for the other velocities. This could be explained by the fact that the major fluid-particle contact area is close to the distributor plate. For low velocities, and with the application of the magnetic field,

Figure 5-7 : Effect of magnetic field on fluid-solid mass transfer for a given bed porosity (ε = 0.79[/])

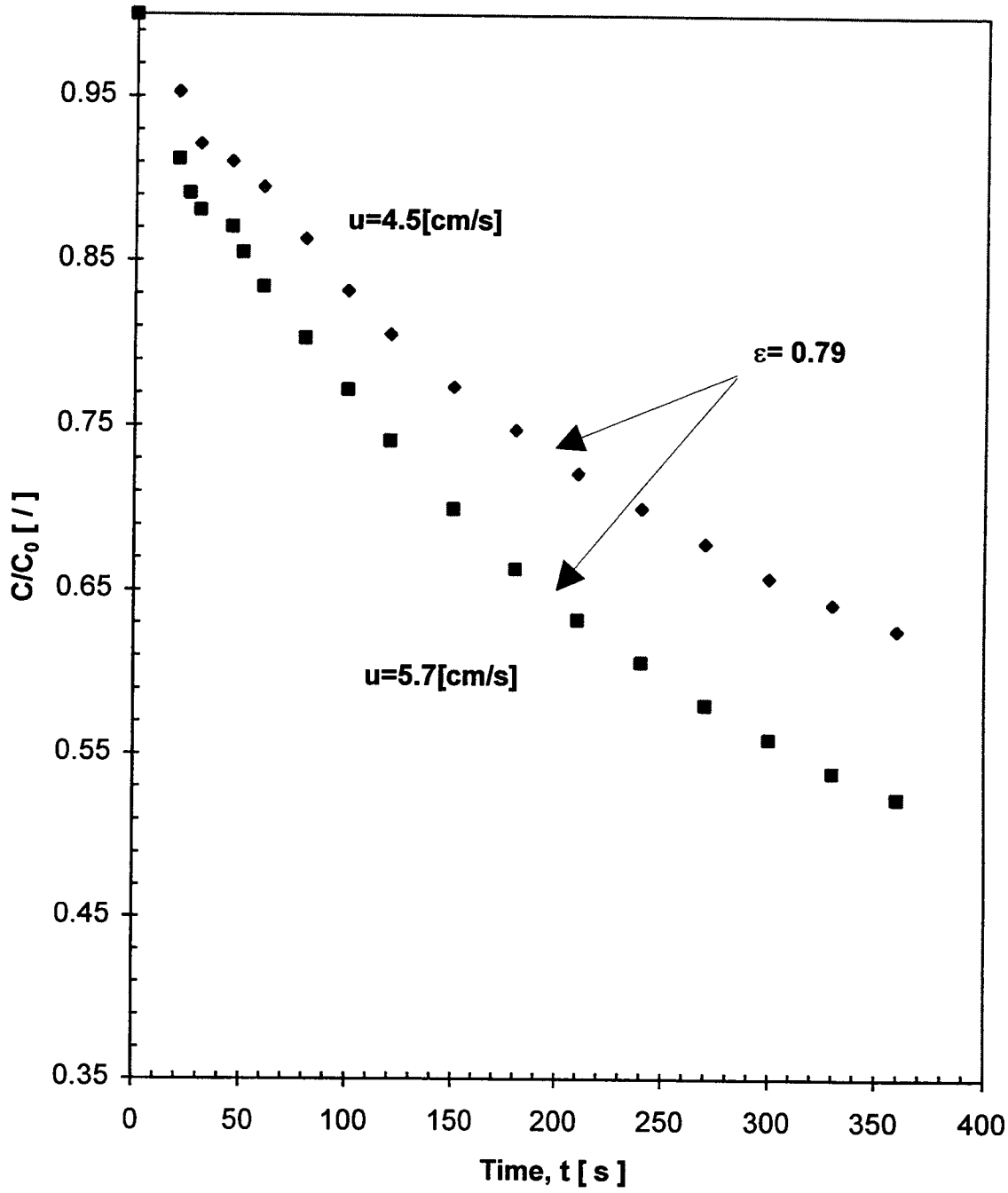

most of the particles are close to the area, where particles experience the effect of fluid jets coming out of the distributor plate. The fluid jets have a very high velocity. We believe that this could have influenced fluid-particle mass transfer. This effect could have substantial effect on the increase of the fluid-particle mass transfer coefficient. To investigate more about the effect of the fluid jets, one should experiment with different distributor plates, which could be done in further studies.

5.3. Mass Transfer Coefficient Correlation :

To evaluate the validity of our measured data, we will correlate our mass transfer coefficient (Sherwood number) with the fluid interstitial velocity, $u_{int.}$ (u_0/ε) . We will use a modified Reynolds number, Re′ that takes into account the fluid interstitial velocity instead of the superficial velocity.

The following parameters are assumed to be constants throughout our experiments :

Fluid kinematic viscosity, $\nu \sim \nu$ of water = 0.01 [cm^2/s]

Diffusivity of MB into water, D =3.6 X 10^{-6} [cm^2/s]

The calculation of diffusivity of MB in water is demonstrated in Appendix J.

We used the correlation (introduced in Chapter 3) proposed by Couderc (1972) as a base for our data fitting.

$$Sh = \frac{0.054}{\varepsilon^2} ReSc^{0.33} \qquad (3\text{-}2)$$

We found that our data can fit reasonably well the equation 3-2. However, our data fit excellently the modified form of equation 3-2, i.e., the constant 0.054 is replaced by 0.0365. The new constant is found by minimizing the sum of the squared differences between the measured and calculated values. Hence our proposed correlation is

$$Sh = \frac{0.0365}{\varepsilon} Re'Sc^{0.33} \qquad (5\text{-}11)$$

Where $$Re' = \frac{\rho u_0 d}{\mu \varepsilon} = \frac{\rho u_0}{\varepsilon \upsilon}$$

Our measured mass transfer coefficient (Sherwood number) values are plotted against the values calculated by equation 5-11. The plot is shown in Figure 5-8.

We were successful in finding a correlation that fits our measured mass transfer coefficient values with the fluid flow properties in MSFB. The correlation obtained is analogous to that proposed by Couderc (1972). The correlation provides a very important factor in designing MSFBs. For a particular mass transfer operation in MSFB, equation 5-11 can predict the bed porosity that yields the desired mass transfer

Figure 5-8 : Plot of the measured against the calculated Sherwood number values

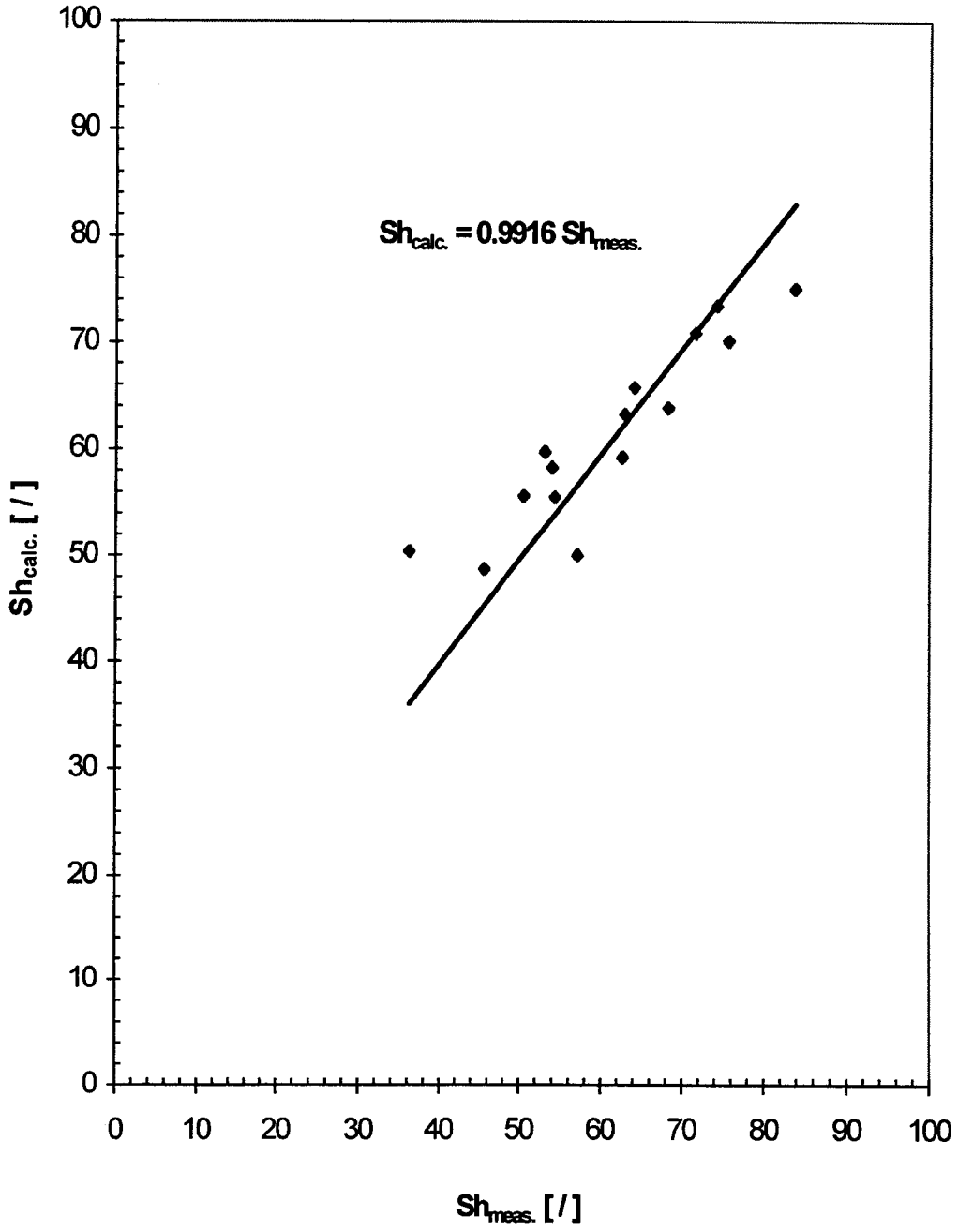

coefficient. Then, using equation 5-1 proposed by Honorez (1994), we can predict the magnetic properties of the particles that should be used in the operation.

CHAPTER 6
CONCLUSION AND RECOMMENDATIONS

6.1. Conclusion

This study is conducted to produce original experimental data for the adsorption of MB dye on ferromagnetic particles in MSFB. Experimental data that relate the bed porosity to the magnetic field intensity in MSFB are also produced. The data are used to calculate and confirm the enhancement of liquid-solid mass transfer coefficient by the magnetic field in MSFB.

In the course of this study a mathematical model is developed that is used to calculate the mass transfer coefficient for the adsorption of MB on the fluidizing particles. The model is solved analytically, and mass transfer coefficient is calculated using the following form of the solution :

$$\mathrm{Ln}\left\{\frac{C(1+mK_e)-C_0}{C_0(1+mK_e)-C_0}\right\}=\frac{1+mK_e}{mK_e}\frac{F}{V}\left(e^{-\alpha k}-1\right)t \qquad (3\text{-}13)$$

Our model solution, and hence our calculation of mass transfer coefficient, is based on the initial adsorption data in which the diffusion resistance is neglected and the particle surface concentration is assumed to be constant.

The equilibrium isotherm that relates the equilibrium concentration of MB in the solution and the amount of MB adsorbed on the particles is found to be linear in the range of our experimental data. The relation obtained is :

$$N = K_e C_s \qquad (4\text{-}2)$$

The trend of the porosity - magnetic field intensity data is found to coincide with the previous studies conducted by Jovanovic et al. (1993) and Honerez (1994). We used the correlation proposed by Honorez (1994) to fit our data, however, equation 5-1 did not fit our data exactly as we expected. Nevertheless this did not interfere with our main objective of evaluating the enhancement of the mass transfer coefficient by the magnetic field.

The most important conclusion of this study is the enhancement of liquid- solid mass transfer coefficient by the magnetic field in MSFB. This is the result that we anticipated earlier because of the increase of the interstitial liquid velocity that results from the application of the magnetic field. The increase of the mass transfer coefficient in MSFB is up to 75 % over that of conventional fluidized bed. The highest increase of mass transfer coefficient is observed for the lowest liquid superficial velocity ($u_0 = 3.2$ [cm/s]). We believe that this is influenced by the effect of the liquid jets coming out of the distributor plate.

A correlation that relates mass transfer coefficient to the interstitial liquid velocity is proposed. :

$$Sh = \frac{0.0365}{\varepsilon} Re' Sc^{0.33} \qquad (5\text{-}11)$$

where $$Re' = \frac{\rho u_0 d}{\mu \varepsilon} = \frac{\rho u_0}{\varepsilon \upsilon}$$

This correlation is analogous to the correlation proposed by Couderc (1972). The fit of our experimental data into equation 5-11 is very convincing.

6.2. Recommendations :

For further studies, the following points are recommended :

1- A rigorous solution to the mathematical model developed in this study could be obtained numerically. It should take into account the diffusion resistance as well as the change of the particle surface concentration throughout the entire adsorption process. However, this requires a reasonable estimate of the internal particle surface, which is not an easy task to do.

2- Experiments with high initial concentrations, where the adsorption isotherm is not linear, should be conducted. Then, a mathematical model based on the non linear isotherm should be developed. Once this is done, along with the previous recommendation, the absolute measurements of the mass transfer coefficient will be more comprehensive.

3- Further studies on higher magnetic field intensities and different magnetic particles should be conducted. Theses studies should evaluate an optimum magnetic field intensity and particle magnetic property that give the maximum liquid-solid mass transfer coefficient in MSFB.

4- The effect of the distributor plate should be investigated rigorously. Different distributor type with various hole sizes should be used in further studies to determine their actual effect on the liquid-solid mass transfer coefficient.

BIBLIOGRAPHY

Arnaldos J. , Casal J., Lucas A., and Puigjaner L., Magnetically Stabilized Fluidization: Modeling and Applications To Mixtuers, ***Powder Technology***, 44,(1985) 57

Ballesteros R. Limas , Riba J.P. and Couderc J.P. , Dissolution oOf Non Spherical Particles In Solid-Liquid Fluidization, ***Chemical Eng. Science,*** 37 (No.11) (1982) 1639

Burns Mark A. and Graves David J., Continous Affinity Chromatography Using a Magnetically Stabilized Fluidized Bed, ***Biotechnology Progress***, 1 (No.2) (1985) 95

Burns Mark A. and Graves David J., Structural Studies Of A Liquid-Fluidized Magnetically Stabilized Bed, ***Chem. Eng. Comm.***, 67 (1988) 315

Casal J. and Arnaldos J., The Structure Of Magnetized Fluidized Beds, ***Powder Technology***, 64 (1991) 43

Chu Ju Chin, Kalil James , and Wetteroth William A. , Mass Transfer In Fluidized Bed, ***Chemical Eng. Progress,*** 49 (No.3) (1953) 141

Filippov M. V., The Effect Of Magnetic Field On A Ferromagnetic Particle Suspension Bed, ***Pric. Magnit. Lat.SSR***, 12 (1960) 215

Furusawa Takehiko and Smith J.M. , Fluid-Particle And Interparticle Mass Transport Rates In Slurries, ***Ind. Eng. Chem. Fundam.***, 12 (No.2) (1973) 197

Honerez Laure, Fluid Dynamic Characteristics of a Magnetically Stabilized Liquid-Solid Fluidized Bed, M.S. Thesis, 1994.

Jovanovic G.N., Sajc L., Jovanovic Z., Vunjak-Novakovic G., Pesic R., and Vukovic D., Liquid Dispersion in Magnetically Stabilized Fluidized Beds, ***Trans. Inst. Chem. Engr.***, 72A (1994) 236

Kunii D. and Levenspiel O., Fluidization Engineering, Wiley, New York (1991)

McKay Gordon, The Adsorbtion Of Dyestuffs From Aqueous Solutions Using Activated Carbon. IV. External Mass Transfer Processes, ***J. Chem. Tech. Biotechnol.***, 33A (1983) 205

McKay Gordon , Murad J. Bino and A. Altememi, External Mass Transfer During The Adsorbtion Of Various Pollutants Onto Activated Carbon, ***Wat. Res.***, 20 (No.4) (1986) 435

Riba J.P. and Couderc J.P., Transfert De Matiere Autour D'une Sohere Immergee Dans Une Couche Fluidisefe Par Un Liquide, ***Int. J.Heat Mass Transfer***, 23 (1980) 909

Rosensweing R.E. , Magnetic Fluidization Of The State Of Uniform Fluidization, ***Ind. Eng. Chem. Fundam.*** , 18 (no 3) (1979) 260

Rosensweing R.E. , Siegell J.H., Lee W.K., and Mikus T. , Magnetically Stabilized Fluidized Solids, ***The American Institute Of Chemical Engineers***, 77 (No. 205) (1981) 8

Sada Eizo, Katoh Shigeo, Shiozawa Masami, and Fukui Tsunehiko, Performance of Fluidized - Bed Reactors Utilizing Magnetic Fields, ***Biotechnology and Bioengineering***, 23 (1981) 2561

Siegell J.H., Liquid-Fluidized Magnetically Stabilized Beds, ***Powder Technology***, 52 (1987) 139

Silem A., Boualia A., Kada R., and Mellah A., Adsorbtion of Organic Matter From a Wet Phosphric Acid Using Activated Carbon: Bach-Contact Time Study and Linear Driving Force Models, ***The Canadian Journal Of Chemical Engineering***, 70 (1992) 491

Singh B., Singh M., Singh S., Singh R., and Lele P.S., Adsorbtion In Fixed and Fluidized Beds, ***Chemical Age OF India***, 14 (No 5) (1963) 395

Tang Li, A Mathematical Model for Adsorbtive Bubble-Seperation Processes, M.S. Thesis, 1990.

Terranova Brenda E. and Burns Mark A., Continuous Cell Suspension Procrssing Using Magnetically Stabilized Fluidized Beds, ***Biotechnology and Bioengineering***, 37 (1991) 110

Tournie P. , Laguerie C. and Couderc J.P., Correlations For Mass Transfer Between Fluidized Spheres And Liquid, ***Chemical Eng. Science***, 34 (1979) 1247

Upadhyay S.N. and Tripathi G., Mass Transfer In Fixed & Fluidized Beds, ***J. Scient. Ind. Res.***, 34 (1975) 10

Vanadurongwan V. , Laguerie C., and Couderc J.P., Influence Des Propri'ite's Physiques Sur Le Transfert De Matiere En Fluidsation Liquide, ***Chemical Eng. J.***, 12 (1976) 156

APPENDICES

APPENDIX A
Preparation Of 500 [g] OF Ferromagnetic Sodium Alginate Solution

1- Weigh a 390 [g] amount of distilled water and place the beaker under the mixer.

2- Weigh a 10 [g] amount of HV sodium alginate powder that will constitute 2% of the total weight of water + alginate.

3- Start mixing the water and add the alginate powder to the water in a small increments away from the mixer until all alginate powder is added to the water.

4- Lit the solution for about 4 to 5 hours. During this time, the solution high viscosity could force the mixer to stop ; consequently, the solution has to be continuously checked over the mixing period.

5- Weigh the amount of ferromagnetic powder that will constitute 20% of the total weight of alginate solution + ferromagnetic powder (100 [g]).

6- Add the ferromagnetic powder to the alginate solution in a small increments while stirring the mixture.

7- Repeat step 6 until all ferromagnetic powder is added and a uniform ferromagnetic alginate solution is obtained.

APPENDIX B
Properties Of Ferromagnetic Powder

The ferromagnetic powder composition is tabulated in Table B-1. The physical and chemical properties of the ferromagnetic powder is tabulated in Table B-2.

Table B-1: Ferromagnetic Powder Components

Component	Chemical Formula	% weight
Manganese Ferrite	($MnOFe_2O_3$)	45-70 %
Zinc Ferrite	($ZnOFe_2O_3$)	25-55 %
Ferrous Ferrite	($FeOFe_2O_3$)	0-0.05 %

Table B-2 : Properties of the ferromagnetic powder

Average Diameter (micron)	2
Surface Area [cm^2 / g]	2.286
Specific Gravity	1.86
Moister %	0.01
Solubility in water	Negligible
Reactivity in water	Negligible
Melting point	> 1500 C
Stability	Stable

APPENDIX C
BEAD GENERATOR DETAILED DRAWINGS

Figure C-1 : Overall structure

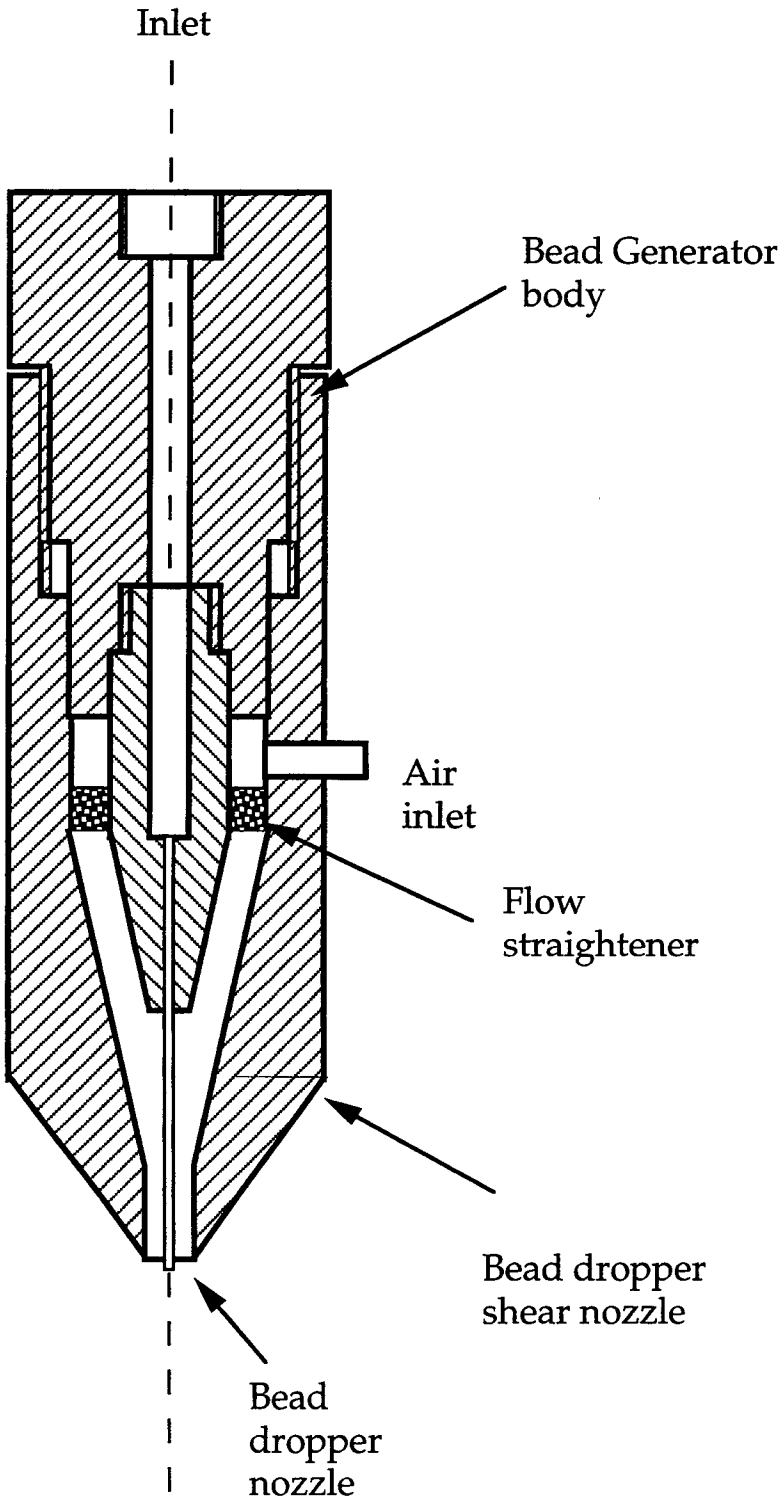

Figure C-2 : Bead generator body

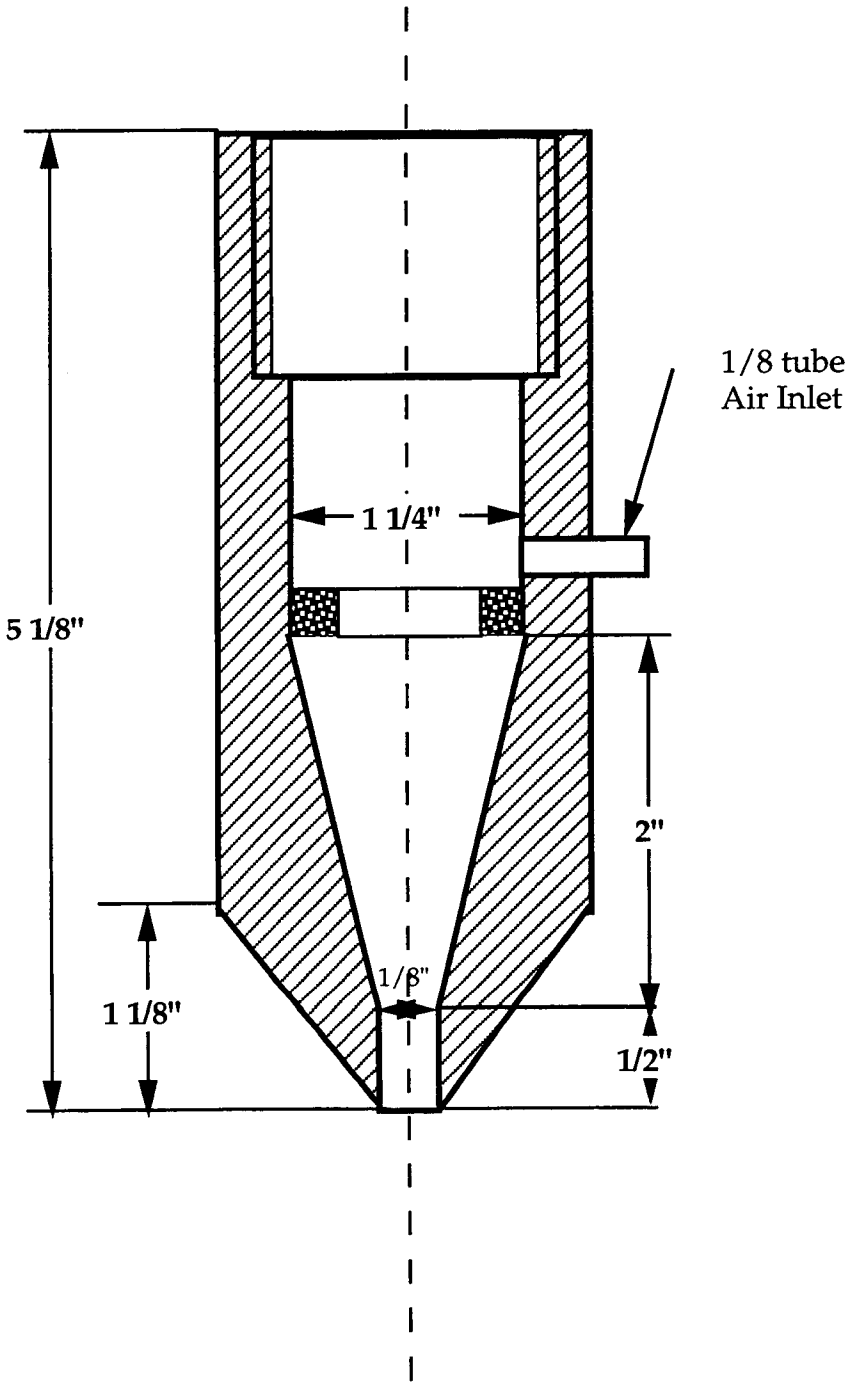

Figure C-3 : Particle generator top portion

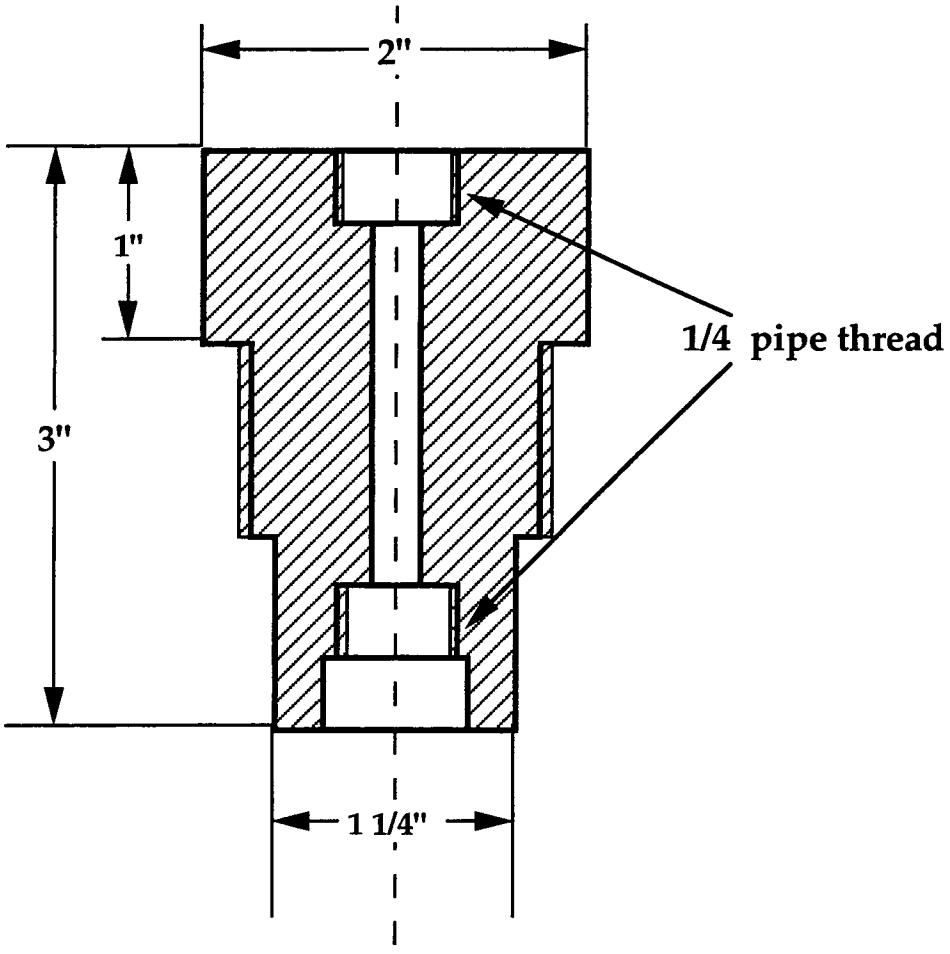

Figure C-4 : Dropper nozzle

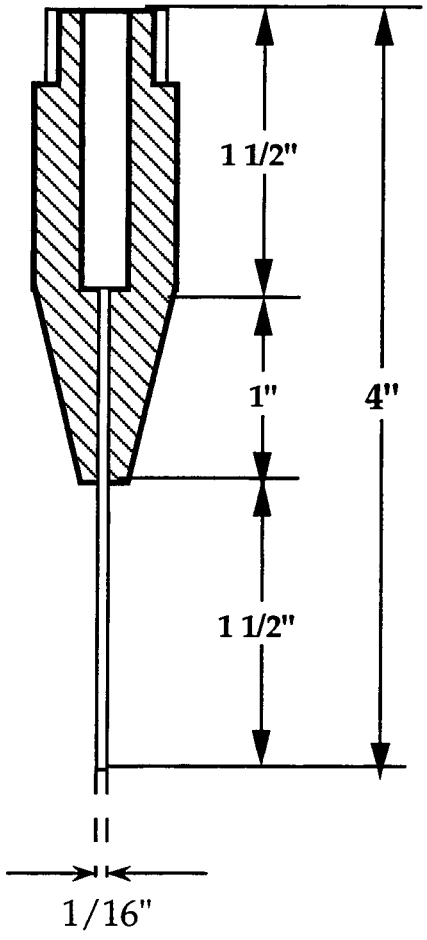

APPENDIX D
STANDARD MAGNETIZATION CURVES

Figure D-1 : [Ferrite content =15%]

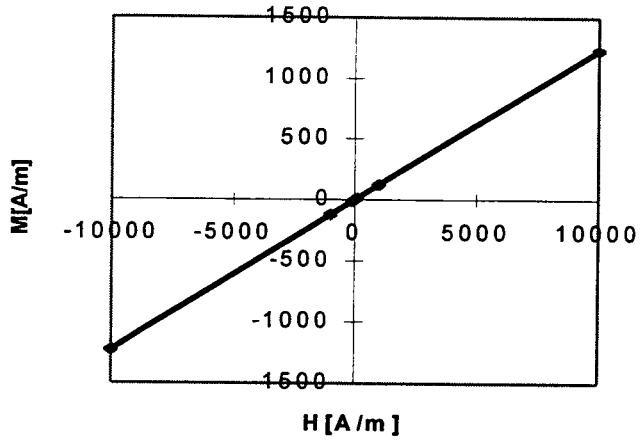

Figure D-2 : [ferrite content =20 %]

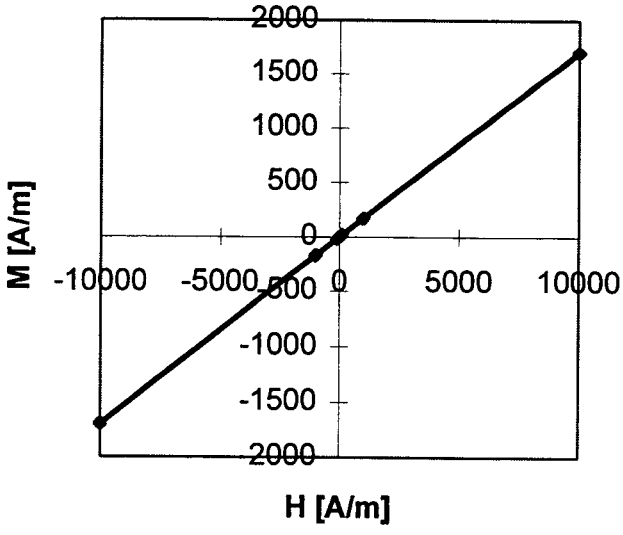

Figure D-3 [ferrite content = 25%]

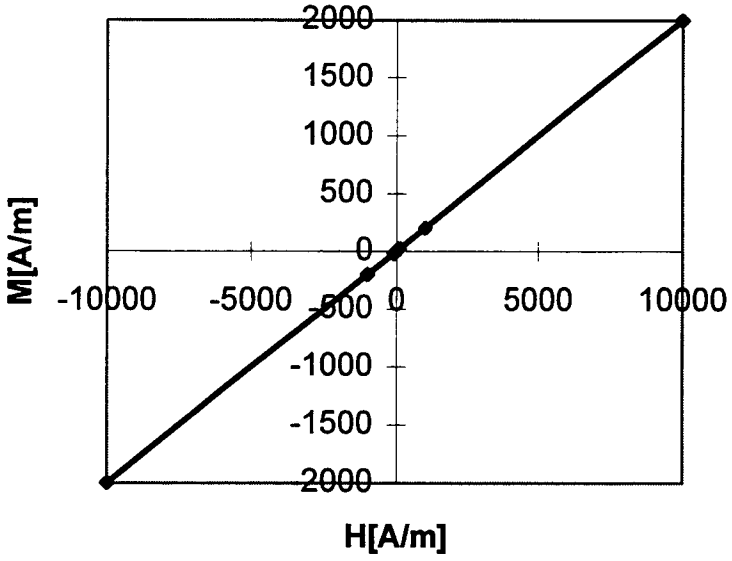

Figure D-4 [ferrite content = 30 %]

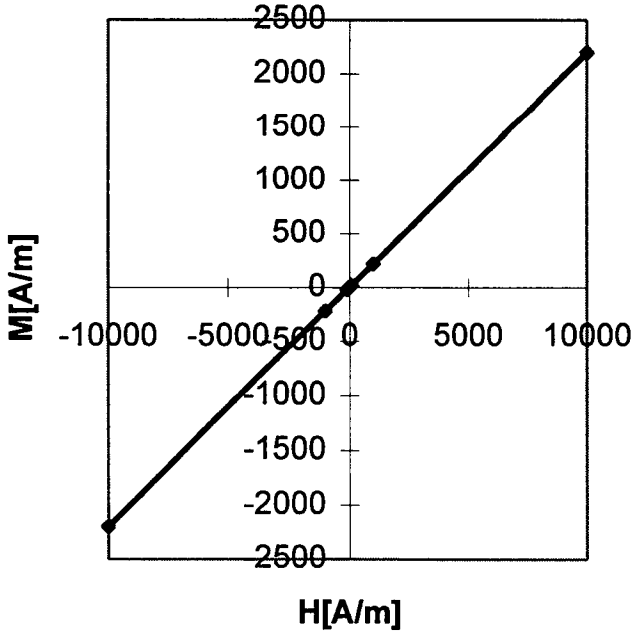

APPENDIX E
CALIBRATION CURVES

Figure E-1 : Flow rotameter calibration curve

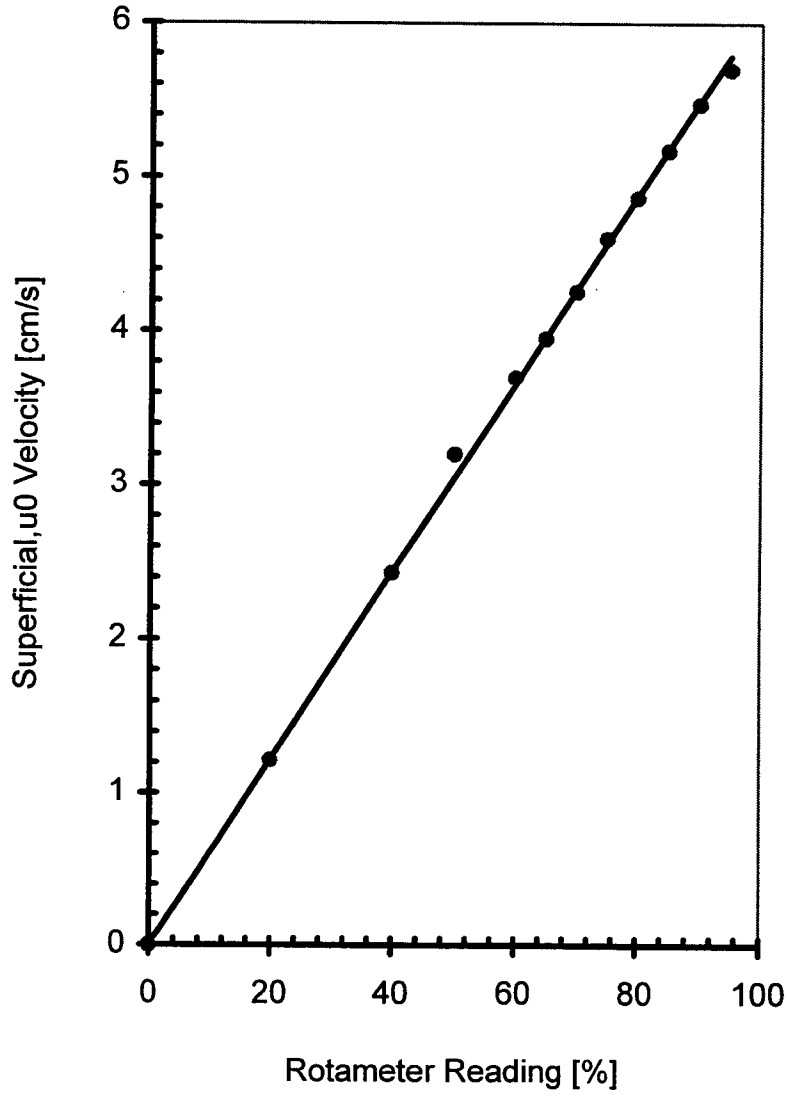

Figure E-2 : Absorbance - concentration calibration curve

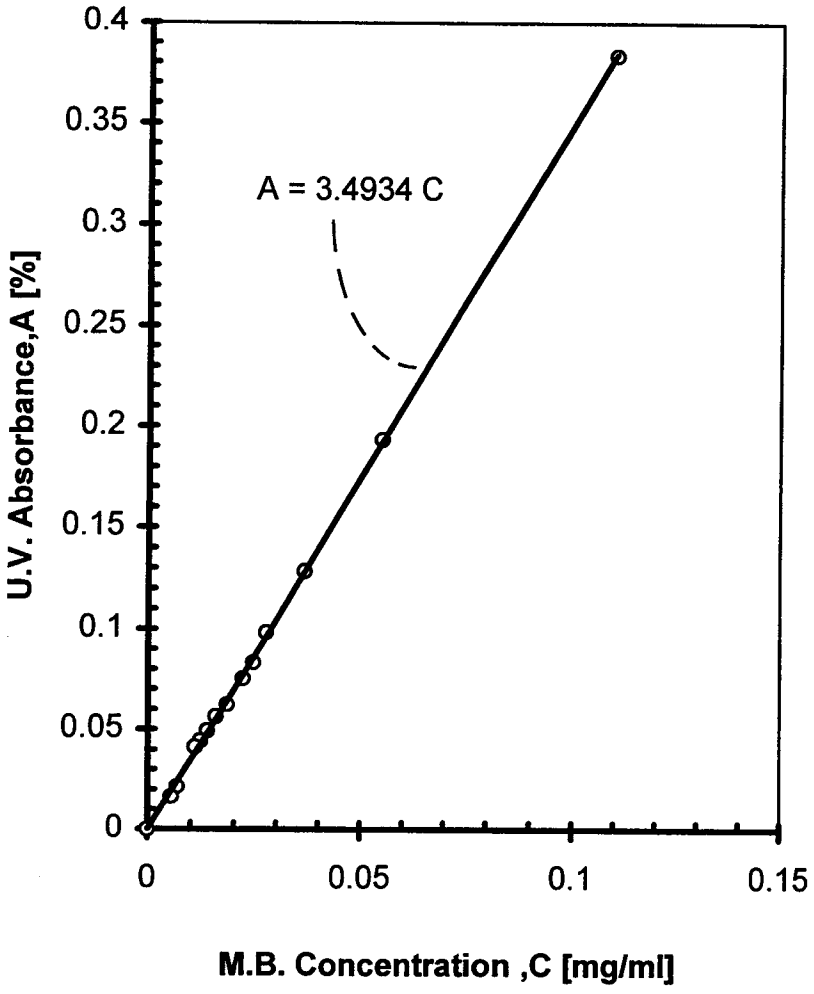

Figure E-3 : Current - voltage calibration curve

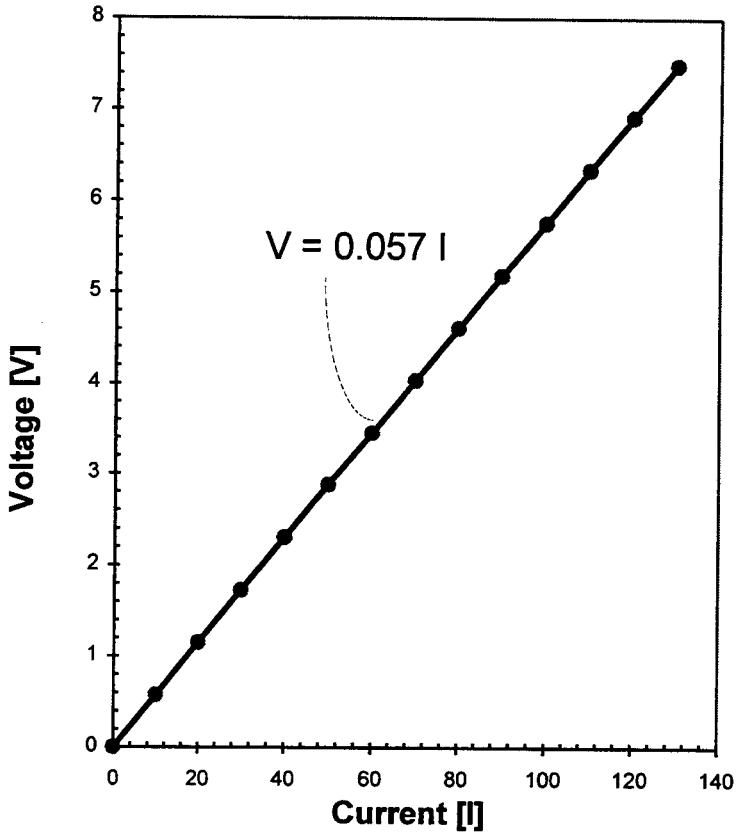

Appendix F
Analytical Solution For Model (1)

From Chapter 3 , the following equation was obtained :

$$\frac{dC}{dC_s} = -mK_e \qquad (3\text{-}14)$$

Integration of Equation 3-12 can be done as :

$$\int_{C_0}^{C} dC = -mK_e \int_{0}^{C_s} dC_s \qquad \Rightarrow$$

$$C_s = \frac{C_0 - C}{mK_e} \qquad (F\text{-}1)$$

Taking into consideration the assumption that C_s is constant during one pass of the fluid through the fluidized bed, equation 3-3 can be integrated throughout the bed height (L) as :

$$\int_{C}^{C'} F\frac{dC}{C - C_s} = -ka'A\int_{0}^{L} dx \qquad \Rightarrow$$

$$Ln\left\{\frac{C' - C_s}{C - C_s}\right\} = -\frac{ka'A}{F}L \qquad (F\text{-}2)$$

Combining equations F-1 and F-2 , we get :

$$\mathrm{Ln}\left\{\frac{C'-\frac{C_0-C}{mK_e}}{C-\frac{C_0-C}{mK_e}}\right\}=-\frac{ka'A}{F}L \qquad \text{(F-3)}$$

Let $\alpha=\frac{a'AL}{F}$, then equation F-3 can be rewritten as :

$$C'=\frac{C_0-C}{mK_e}+\left\{C-\frac{C_0-C}{mK_e}\right\}e^{-\alpha k} \qquad \text{(F-4)}$$

By combining equation F-4 with equation 3-1, we obtain :

$$F\left\{C-\frac{C_0-C}{mK_e}\right\}\left\{e^{-\alpha k}-1\right\}=V\frac{dC}{dt} \qquad \text{(F-5)}$$

Equation F-5 can be rearranged as :

$$C(1+mK_e)-C_0=\left(\frac{V}{F}\right)\left\{\frac{mK_e}{e^{-\alpha k}-1}\right\}\frac{dC}{dt} \qquad \text{(F-6)}$$

Equation F-6 can be integrated to account for the total adsorbate concentration change throughout the system as :

$$\int_{C_0}^{C} \frac{dC}{C(1+mK_e)} = \frac{F}{V}\left\{\frac{\left(e^{-\alpha k}-1\right)}{mK_e}\right\}\int_0^t dt \qquad \text{(F-7)}$$

Equation F-7 can be integrated easily to obtain the final form as equation 3-15.

$$\text{Ln}\left\{\frac{C(1+mK_e)-C_0}{C_o(1+mK_e)-C_0}\right\} = \frac{1+mK_e}{mK_e}\frac{F}{V}\left(e^{-\alpha k}-1\right)t \qquad \text{(3-15)}$$

To check our solution, as $t \rightarrow 0$, the right hand side of equation (3-15) $\rightarrow 0$, which leads to :

$$C(1+mK_e)-C_0 = C_0(1+mK_e)-C_0 \Rightarrow$$

$C = C_0$, which satisfies BC3.

As $t \rightarrow \infty$, then the right hand side of equation (3-13) $\rightarrow -\infty$ because k and α are always positive. This leads to :

$$C(1+mK_e)-C_0 = 0 \qquad \Rightarrow$$

$$C = \frac{C_0}{1 + mK_e} = C_s$$

which is the result we expect if the adsorption process proceeds to an infinite time period.

APPENDIX G
Analytical Solution For Model(2)

Equations 3-1 and 3-5 are combined to give :

$$\frac{dC}{dt} = -ka'\left(C + \frac{C - C_0}{mK_e}\right) = -ka'\frac{CmK_e + C - C_0}{mK_e} \qquad \text{(G-1)}$$

Equation G-1 is integrated as :

$$\int_{C_0}^{C} \frac{dC}{C(mK_e + 1) - C_0} = -\frac{ka'}{mK_e}\int_0^t dt \qquad \text{(G-2)}$$

which yields :

$$\text{Ln}\left\{\frac{C(mK_e + 1) - C_0}{C_0(mK_e + 1) - C_0}\right\} = \frac{mK_e + 1}{mK_e} ka't \qquad \text{(G-3)}$$

Equation G-3 can be rearranged as :

$$\text{Ln}\left\{\frac{\frac{C}{C_0}(mK_e + 1) - 1}{mK_e}\right\} = -\frac{mK_e + 1}{mK_e} ka't \qquad \text{(G-4)}$$

or, in other form :

$$\frac{C}{C_0} = \frac{1}{1+mK_e} + \frac{mK_e}{1+mK_e} \exp - \left\{ \left(\frac{1+mK_e}{mK_e} \right) ka't \right\} \qquad \text{(G-5)}$$

Equations G-4 and G-5 represent two different forms for the final solution to model(2).

APPENDIX H
Simplifications For Model(1) and Model(2)

Model(1) can be simplified further if we assume that at the beginning of the adsorption process the surface concentration C_s=0. Then, equation F-2 can be simplified to :

$$\mathrm{Ln}\left(\frac{C'}{C}\right) = -\frac{ka'A}{F}L \qquad \text{(H-1)}$$

which leads to :

$$C' = Ce^{-\alpha k} \qquad \text{(H-2)}$$

Combining equation 3-1 with equation H-2 leads to :

$$FC\left(e^{-\alpha k} - 1\right) = V\frac{dC}{dt} \qquad \text{(H-3)}$$

Equation H-3 is integrated as :

$$\int_{C_0}^{C} \frac{dC}{C} = \frac{F}{V}\left(e^{-\alpha k} - 1\right)\int_0^t dt \qquad \text{(H-4)}$$

The integration leads to equation 3-17.

Model(2) also could be simplified further if we incorporate the assumption that C_s=0 into the overall adsorbate concentration change equation (equation 3-5), then we only have to evaluate this integral :

$$\int_{C_0}^{C} \frac{dC}{C} = -ka' \int_{0}^{t} dt$$

which leads to the final simplified form of model(2)(equation 3-18).

APPENDIX I
MB Concentration Measurment Data

Table I- 1: MB concentration measurements for fluid velocity, u_0 =3.2 [cm/s]

Time, T [s]	C/C_0 H=0 [kA/m] A_0=0.131 [%]	C/C_0 H=3.3 [KA/m] A_0=0.18 [%]	C/C_0 H=6.1 [KA/m] A_0=0.17 [%]
0	1	1	1
20	0.992	0.961	
30		0.95	0.935
40	0.969	0.928	0.906
50		0.894	0.876
60	0.938	0.867	0.959
90	0.915	0.822	0.806
120	0.892	0.772	0.759
150	0.877	0.733	0.718
180	0.862	0.694	0.677
210		0.656	0.647
240	0.831	0.627	0.612
270	0.815		
300	0.808	0.572	0.565
330	0.800		
360	0.792	0.528	0.518

Table I- 2 : MB Concentration measurement for fluid velocity, u_0 =3.7 [cm/s]

Time, T [s]	C/C_0 H=0 [kA/m] A_0=0.130 [%]	C/C_0 H=6.1 [kA/m] A_0=0.166 [%]	C/C_0 H=8.3 [kA/m] A_0=0.145 [%]
0	1	1	1
20	0.985	0.982	0.959
25		0.964	
30	0.969	0.952	0.931
35		0.934	
40	0.947	0.922	0.897
45		0.916	
50	0.931		0.876
55		0.904	
60		0.898	0.869
80		0.855	
90	0.901		0.807
100		0.825	
120	0.878	0.795	0.766
150	0.863	0.765	0.717
180	0.840		0.683
210	0.824	0.699	0.648
240	0.817	0.675	0.614
270	0.802	0.651	
300	0.794	0.627	0.572
330	0.779	0.620	
360	0.771	0.602	0.538

Table I- 3 : MB concentration measurements for fluid velocity, u_0=4.5 [cm/s]

Time,T [s]	C/C_0 H=0 [kA/m] A_0=0.131 [%]	C/C_0 H=5.5 [kA/m] A_0=0.190 [%]	C/C_0 H=8.8 [kA/m] A_0= 0.13 [%]	C/C_0 H=13.2 [kA/m] A_0=0.168 [%]	C/C_0 H=14.3[kA/m] A_0=0.124 [%]
0	1	1	1	1	1
10	0.977				0.992
20	0.938	0.953	0.969	0.952	0.960
25				0.929	
30	0.900	0.921	0.939	0.911	0.927
35				0.905	
40	0.885		0.924	0.899	0.903
45		0.910		0.893	
50	0.877		0.924	0.887	0.895
55				0.881	
60	0.869	0.895	0.916	0.869	0.879
70	0.846				0.863
80	0.831	0.863		0.827	0.847
90	0.823		0.878		0.839
100	0.815	0.832		0.804	0.815
110	0.800				0.798
120	0.785	0.805	0.847	0.768	0.782
150	0.754	0.774	0.824	0.732	0.766
180	0.731	0.747	0.809	0.696	0.742
210	0.700	0.721	0.786	0.661	0.718
240	0.677	0.700	0.771	0.637	0.702
270	0.654	0.679	0.756	0.607	0.685
300	0.631	0.658	0.748	0.589	0.669
330	0.615	0.642	0.733	0.565	0.661
360	0.608	0.626	0.725	0.542	0.653

Table I- 4 : MB concentration measurement for fliud velocity, u_0 =5.7 [cm/s]

Time, T[s]	C/C_0 H=0 [kA/m] A_0=0.167 [%]	C/C_0 H=8.8 [kA/m] A_0=0.131 [%]	C/C_0 H=10.97 [kA/m] A_0=0.193 [%]	C/C_0 H=14.3 [kA/m] A_0=0.131 [%]
0	1	1	1	1
10		0.969		
20	0.946	0.931	0.912	0.939
25	0.922			
30	0.910	0.885	0.881	0.885
35	0.898			
40	0.892	0.878		0.84
45	0.886		0.87	
50	0.874	0.863		0.817
55	0.862			
60	0.856	0.84	0.834	0.779
70		0.817		
80			0.803	
90		0.787		0.763
100	0.790	0.771	0.772	
110		0.756		
120	0.760	0.740	0.741	0.748
150	0.719	0.695	0.699	0.710
180	0.689	0.664	0.663	0.679
210	0.659	0.633	0.632	0.641
240	0.629	0.603	0.606	0.618
270	0.605	0.580	0.580	0.588
300	0.581	0.557	0.559	0.573
330	0.563	0.534	0.538	0.55
360	0.545	0.519	0.523	0.534

Appendix J
Calculation of the Diffusivity of MB. Into Water

We use Wilke and Chang (1955) equation for the calculation of the diffusion coefficient of species A present in low concentration in species B. In our case, A represents MB. and B represents water. The equation is :

$$D_{AB} = 7.4x10^{-8} \frac{\sqrt{\phi_B M_B} T}{\mu_B V_A^{0.6}} \qquad \text{(J-1)}$$

where :

ϕ_B is the association factor for water = 2.26 [/]

M_B is the molecular weight of water = 18 [g/mol]

T = 298 [K]

μ_B is water viscosity = 1.0 [Mpa.s]

V_A is the molar volume of MB = 457.1 [cm^3/mol]

Substituting the above values into equation J-1 yields :

$$D_{AB} = 3.6 \times 10^{-6} \quad [\ cm^2/s\ ]$$